AVCO TULSA

THIS DOCUMENT CONSISTS OF PAGES

THIS IS COPY NO. OF COPIES

STUDY OF THE CORRELATION BETWEEN LINEAR ENERGY TRANSFER AND RELATIVE BIOLOGICAL EFFECTIVENESS

Final Report
Contract NASw-782
July 1963 - August 1964

THIS REPORT PREPARED FOR

National Aeronautics and Space Administration
Washington, D. C.

AVCO TULSA

P.O. Drawer N, Admiral Station Tulsa, Oklahoma
Area Code 918 TEmple 5-6911

FOREWORD

This is the final report for work performed on NASA contract NASw-782 entitled "Study of the Correlation Between Linear Energy Transfer and Relative Biological Effectiveness." The program was administered under the direction of the Office of Advanced Research and Technology of the National Aeronautics and Space Administration with Dr. Leo Fox and Dr. George Chatham the project monitors.

The experimental studies were completed as a result of joint effort by Avco/Tulsa and the Oklahoma University Research Institute (OURI) during the period July 1963 to August 1964. The work was conducted at the Avco Biophysics Research Laboratory located on a campus of the University of Oklahoma. Mr. K. M. Hoalst of Avco/Tulsa was program manager for the research activity.

The instruments for this program were designed by Mr. Joseph F. Tinney of Avco/Tulsa and the theoretical application of the measurement parameters was conducted by Mr. Tinney and Dr. Jack Cohn of OURI. Mr. Clifton A. Aldridge of Avco/Tulsa and Dr. J. Bennett Clark of OURI developed the biological system for the program and performed all subsequent biological work. Mr. Keith Warble of Avco/Tulsa designed the electronics and assisted with the off-site experiments. Mr. Gordon Kramer of Avco/Tulsa was responsible for the first off-site experiment and Messrs. Aldridge, Tinney and Warble conducted all subsequent off-site experiments.

TABLE OF CONTENTS

ABSTRACT

29573

Instrumentation and biological systems have been developed to study the correlation between linear energy transfer (LET) and relative biological effectiveness (RBE). The instruments developed for this program include small tissue equivalent proportional counters for measuring LET spectra over a wide range of radiation intensities; and tissue equivalent ionization chambers for the direct measurement of radiation absorbed dose in tissue.

In the biological system development, living tissue was simulated by compacting haploid yeast cells (strain Sc-7) in solid polyethylene glycol. The compacted mass of cells was irradiated and serial sections were taken to assay radiation damage at various depths. The ability of the irradiated cells to produce a macroscopic colony on suitable nutrient material was a measure of cell survival.

Radiation exposures were made with 22.3 Mev and 210 Mev protons, and the results were compared with 200 KVCP x-ray irradiation results.

The slopes of the yeast cell survivors versus absorbed dose curves were found to be directly related to average LET, as has been reported by other workers.

It is felt that a significant biological tool has been developed which could be used for radiation additivity studies, microbeam radiation damage studies, and other related research problems.

The results presented in this report also indicate that the radiation quality sensors developed for this program could be used to examine the radiation environment in space.

Author

I. INTRODUCTION

Manned spaceflights are placing increasing emphasis on the need for the development of instrument systems for measuring biologically significant properties of the space radiation environment. In fact, tissue equivalent ionization chambers for measuring total absorbed dose from ionizing space radiations have already been developed and flown in deep space probes and satellites.[1,2] Instruments of this type are also being fabricated for use in future manned and unmanned space explorations.[3] However, numerous laboratory experiments[4,5] have shown that the biological effectiveness of radiation depends not only upon the total amount of energy absorbed, but also upon the "quality" of the radiation, the biological system and effect studied, the environment, and the physiological state of the system. The primary purpose of this research program has been to develop an instrument for measuring radiation "quality," and to correlate the results of these measurements with the radiation damage effects on a suitable biological system. Since space radiations include protons, electrons, x-rays, and cosmic rays[6], it is important that the sensor measure a radiation quality that is characteristic of all types of radiation and is directly related to biological response.

Historically, radiation quality has been expressed as a distribution of dose in linear energy transfer (LET), specifying the fraction of the dose deposited in each LET interval.[7] The results of numerous laboratory experiments have substantiated the variation of biological response with this parameter. However, Rossi[7] has pointed out limitations of the concept which indicate that it is very difficult to measure LET spectra in an unknown radiation environment. To overcome these limitations, Rossi has proposed the concepts of 'Y' and 'Z' as alternate characterizations of radiation quality. The parameter Y is defined as the energy imparted to a small sphere divided by the sphere diameter. Representation of the dose in Y for a range of diameters yields information on the spatial distribution of energy, as well as on the local dose and the frequency with which such a dose is delivered. The parameter Z is defined as the energy absorbed per unit mass in the volume being investigated. Y and Z can both be measured for radiation fields with unknown physical characteristics and could be used to specify the quality of space radiations.

The ultimate test of any physical system designed for measuring radiation quality is the comparison of the measured properties of the radiation field with biological effects. A large number of biological systems have been used for this type of work; and, therefore, the choice of biological system is defined to some degree by the conditions or objectives of the experiment.

This report describes the design and development of a Y sensor, based on Rossi's original concepts, that can be ruggedized for spaceflight. Presented also are the results of an extensive accelerator program conducted to calibrate the sensor and correlate the results with the response of a suitable biological system.

II. EXPERIMENTAL PROCEDURE AND INSTRUMENTS

A. Biological

In developing the biological system to be used in correlative studies with the instruments developed in these laboratories, the following criteria were established:

1. The system should allow a maximum accuracy in quantitation of biological effects.

2. The system should allow depth-dose studies to be made under conditions similar to those obtained in tissue.

3. The system should have biological stability in order to allow the time delay inherent in preparing the system in the laboratory, irradiating the system at a source which may be hundreds of miles away, and returning the system to the laboratory for testing after irradiation.

The system finally developed was composed of the Sc-7 strain of yeast embedded in polyethylene glycol. Although this organism was not as LET sensitive as some other cells, it had the advantage of voluminous previous work reported in the literature. Other cells were investigated such as Bacillus megaterium spores and Artemia eggs, but the main work was done with the yeast cells.

Polyethylene glycol was the best embedding material found. It was nontoxic and allowed biological stability. It was essentially tissue equivalent and for precise depth dose studies, it could be accurately sectioned with a microtome in slices as thin as 10 microns. The mixture used melts at 40°C and is water soluble, thus allowing easy embedding and release of the cells after sectioning.

Other embedding materials were tested but discarded as being inferior to polyethylene glycol. These included frozen gelatin, agar-agar, various gums and low melting point paraffins. Also various combinations of different molecular weight polyethylene glycol preparations were tested.

Procedure

The procedure for constructing the biological system was as follows: a quarter inch constant diameter bore was made in paraffin contained in a 50 ml test tube. The bore was about three inches in depth.

The melted polyethylene glycol was mixed in the following ratio: 20 ml having an average molecular weight of 1500 with 2 ml of average molecular weight 4000.

The mixture was then cooled in a water bath to 42°C. Two grams of wet yeast cells (washed five times and packed to a paste by centrifugation) were then stirred into the mixture until the cells were evenly dispersed. This treatment was performed in a 42°C water bath to prevent hardening of the mixture. The cell suspension was then poured into the wax mold and packed by clinical type centrifuge (no angle head) which allowed the cells to pack into the bore. After proper trimming, the resulting compacted mass of cells contained in the paraffin mold (referred to as an ingot), was ready for irradiation.

Through experience, it was shown that about 3 cm of the packed cell mass could be used; that is, reproducible results could be obtained with 10 micron slices through 3 cm of the packed cells.

It was found that when too much high molecular weight polyethylene glycol was added, the cell mass became too brittle to slice. When none was added, the mixture remained too waxy and could not be sliced thinner than 50 microns.

Stability of Embedded Cells

The decay rate of the viable count for haploid yeast in polyethylene glycol is sufficiently small to allow fabrication of the tissue simulant several days prior to its use.

Direct microscopic counts of the total number of cells present were made using a Petroff-Hausser counting chamber. Total counts from 100 micron slices of the compacted yeast cell mass were compared to viable cell counts obtained from 100 micron slices from the same unirradiated ingot which had been transported to and from the accelerator site. The result of averaging five determinations indicated that 39 percent of the cells were still viable after three days. Viability counts of the yeast cell paste used to fabricate the tissue simulant ingots, compared to total counts of the same paste, gave a value of 83 percent. Thus, of the 83 percent viable cells used to fabricate the yeast cell mass, 44 percent were surviving after three days storage in polyethylene glycol.

This decay rate is well within statistically useful limits. These results further indicate that interpretation of radiation damage to the yeast cell mass is applied to the greater population of yeast cells rather than a select few.

Toxicity and Dehydration Effect of Polyethylene Glycol

Yeast toxicity studies with polyethylene glycol irradiated with 22.3 Mev protons failed to demonstrate any toxic products formed for dosages up to 30,000 rad.

Preliminary data collected with the completed experimental system after x-irradiation indicated that the dehydrating effect of polyethylene glycol had a protective effect and comparisons with 200 KVCP x-ray killing curves obtained from wet cells were invalid. Accordingly, killing curves for the haploid yeast cells in polyethylene glycol were obtained from data collected after irradiating different ingots of the compacted cells. (Figure 1)

Oxygen Effect

Experiments in which the yeast ingots were irradiated with protons or x-rays always revealed an increased killing rate at the front of the ingot. It was thought that this increased killing might be caused by oxygen diffusing into the first five millimeters of the yeast mass.[14,18] This could cause an increased sensitivity due to the oxygen effect.

In order to evaluate this possibility, ingots of yeast cells were prepared in the usual manner. Several of the ingots were immediately placed in an atmosphere of flowing nitrogen gas. After a minimum of two hours standing in the nitrogen atmosphere, the ingots were irradiated in a nitrogen atmosphere. Other ingots were handled in the usual manner in which they were exposed to air for varying lengths of time. The ingots maintained and irradiated in nitrogen showed no increased killing at the front of the ingot. Those ingots exposed to air consistently demonstrated the increased killing.

Tissue Equivalency of Polyethylene Glycol

The following data and information are compiled to show tissue equivalency of the polyethylene glycol mixture used in these experiments. Polyethylene glycol had a generalized chemical formula of $HOCH_2(CH_2 OCH_2)_n$ where n indicates the degree of polymerization. The mixture used in these experiments had a molecular weight of 1540; therefore, n equals 34. Consequently, the chemical formula is

$$H_{9.1}C_{4.5}O_{2.3}$$

where the subscripts indicate the number of each element per 100 gms of polyethylene glycol. The fraction by weight of each element is

$$H_{0.091}C_{0.542}O_{0.367}$$

and the total mass-energy absorption coefficient is obtained by the following equation:

$$\begin{aligned}(m\ \ ev)_{total} &= 0.091\,(m\ \ ev)_H \\ &+ 0.542\,(m\ \ ev)_C \\ &+ 0.367\,(m\ \ ev)_O\end{aligned}$$

Values for (m ev) are obtained from Table 8.1 of NBS Handbook 78, and Table I is a tabulation of the calculated values divided by values for (m ev) muscle provided in the same table.

Photon Energy Mev	(m ev) carbowax / (m ev) muscle	Percent Error
.010	0.68	38.0
.020	0.60	40.0
.030	0.61	39.0
.050	0.70	30.0
.080	0.905	9.5
.100	0.948	5.2
.200	0.985	1.5
.500	0.99	1.0
1.0	0.985	1.5
2.0	0.99	1.0
5.0	0.983	1.17
10.0	0.960	4.0

Table I: A Comparison of Photon Mass-Energy Absorption Coefficients of Polyethylene Glycol with Muscle.

Maximum error occurs in the low energy region where the photoelectric effect predominates. At higher energies, the Compton effect takes over and here the error is small. This is to be expected since the Compton absorption of each atom is proportional to its atomic number, hence, to the total number of electrons per gm of material. For the composition of muscle tissue adopted by the International Commission of Radiological Units, i.e., $C_{1.024}H_{10.2}O_{4.556}N_{0.25}Na_{0.0035}Mg_{0.0008}P_{0.0065}S_{0.0156}K_{0.0077}Ca_{0.0017}$, this quantity is 55.087 mole-electrons/100 gms. For polyethylene glycol, the quantity is 54.5 mole-electrons /100 gms. Thus, the ratio of energy absorbed per gm from Compton effect is 54.5/55.087 = 0.988, or an error of 1.2 percent which agrees well with that calculated for the range of photon energies between 0.20 Mev and 5 Mev.

B. Dosimetry

The tissue equivalent ionization chambers used for this experiment were a modification of instruments that were developed for the Air Force.[2] Measurements made with these instruments provide a direct indication of the tissue absorbed dose and a detailed knowledge of the incident radiation spectrum is not required. The following is a discussion of the concepts involved in the measurement of radiation absorbed dose and a description of the modified instruments.

The most convenient method for measurement of radiation energy absorbed by a given material is through the use of the Bragg-Gray relation. The basic conditions necessary for the use of this relationship are summarized as follows:

1. The cavity must have dimensions such that only a very small fraction of the particle energy is dissipated in it. This means also that only a very small fraction of the particles contributing to the ionization will enter the cavity with a range smaller than the cavity dimensions.

2. Direct absorption of quantum radiation by the gas in the cavity should contribute only a negligible proportion of the total ionization.

3. The cavity must be surrounded by an "equilibrium thickness" of the solid medium so that all particles crossing it originate in the medium.

4. The energy dissipation by the ionizing particles must be uniform over the volume of the medium immediately surrounding the cavity and contributing to the electronic equilibrium.

If the gas and the surrounding medium are of identical atomic composition, the cavity can be large without disturbing the flux of secondary particles. Or, according to Fano's theorem: "In a medium of given composition exposed to a uniform flux of primary radiation, the flux of secondary radiation is also uniform and independent of the density of the medium, as well as of the density variations from point to point."

Thus, the cavity ionization principle permits a determination of energy absorption in a solid medium from the measured ionization in a small gas-filled cavity. This principle was the basis of the energy deposition dosimetry in this program.

The ionization chambers were constructed of a tissue equivalent conducting plastic developed by Shonka[8] which reproduces the tissue absorption coefficients as recommended by the International Commission of Radiological Units within small errors. (See Figures 2 and 3). In addition to being tissue equivalent, this material is rigid, durable, and impervious to and free from chemical attack by certain tissue equivalent filling gases. Table II is a tabulation of the chemical formulation indicated as percentage by weight of this plastic and other tissue equivalent materials surveyed as a part of this program.

Since the ionization chambers were used for measuring rads in a tissue equivalent medium, both the chamber wall and the gas were matched to the medium. The nonexplosive tissue equivalent gas filling was the mixture of methane, carbon dioxide, and nitrogen presented in Table II. Observations of the gamma and neutron sensitivity of a tissue equivalent ionization chamber using this filling gas have indicated a stability within the measuring accuracy of $\pm$ 2 percent over a period of more than six months, thus indicating that no measurable change in the filling gas has occurred through diffusion or absorption losses in the cavity wall during this time.[9]

Since the chambers had tissue equivalent walls and gas filling, they could be exposed to precisely known quantities of hard x- or gamma-radiation for calibration. However, allowance for the change in response due to the difference in W (the energy expended in the production of an ion pair) for electrons and protons,[10,11] as indicated in Table III, must be made.

To relax the requirements of stability on the high voltage power supply and to simplify the calibration procedure, the chambers were operated on the plateau of the ionization curve.

Element	Alderson (% by weight)	Shonka (% by weight)	Markite (% by weight)	Polyethylene (% by weight)	Tissue Equivalent Gas (% by weight)
Carbon	68.803	12.3	86.4	86.5	45.6
Hydrogen	8.891	10.2	5.6	10.0	10.1
Oxygen	22.181	73.0	4.3		40.8
Nitrogen	3.150	3.5	3.7	3.5	3.5
Magnesium	0.034	0.02			
Iron	0.005				
Sulfur	0.280	0.2			
Potassium	0.172	0.5			
Sodium	0.094	0.05			
Phosphorus	0.268	0.2			
Chlorine	0.122				
Calcium		0.03			

Table II : Compositions of Various Tissue Equivalent Plastics and Gases

Gas	Formula	W, Electrons x-rays and γ-rays	W Protons	W, Alpha Particles
Carbon Dioxide	CO_2	33.0 ± 0.5	34.9 ± 0.5	34.2 ± 0.7
Methane	CH_4	22.7 ± 0.9	.....	29.4 ± 0.8
Nitrogen	N_2	34.8 ± 0.5	36.6 ± 0.5	36.4 ± 0.4
Tissue	30.01% CO_2	.....	30.5 ± 0.4	.....
Equivalent	1.74% N_2	Percent by partial pressure		
Gas	67.92% CH_4			
	0.33% C_2H_6			

TABLE III : The Energy Expended in the Production of an Ion Pair in Various Gases for Electrons, Protons, and Alpha Particles.

Calibration of the ionization chambers was performed using heavily filtered 200 KVCP x-rays (HVL - 1.29 mm Cu) and accurately calibrated Victoreen R-meters. The geometry for these calibrations was such that radiation scattered into the measuring region was minimized. A typical calibration curve is presented in Figure 4. All current measurements were made with a Keithley electrometer that was calibrated before and after each experiment.

C. Radiation Quality Measurements

The radiation quality sensors developed as a part of this experimental program were based on design concepts originally proposed by Rossi. The instruments are basically proportional counters with tissue quivalent plastic walls and tissue equivalent filling gas. To measure LET spectra and Y spectra for a wide variety of radiations, both cylindrical (parallel plate) and spherical chambers were fabricated. The cylindrical proportional counters have very thin entrance windows and were used to measure LET spectra (from which Y spectra were calculated) produced by unidirectional beams with low penetrating power. The spherical chambers, on the other hand, were designed to measure Y spectra produced by high energy particle beams, neutrons, x- and gamma-rays and unknown radiation fields. If the directional properties of the radiation field are known, the relationship between LET and Y spectra can be expressed by the following equation.[7]

$$D(\bar{Y}) = 3\,Y^2 \int_{Y}^{L_{max}} D(L)\,\frac{dL}{L^3}$$

The spherical proportional counter developed for this program is illustrated in Figure 5. The sensitive volume of the counter was a 0.5 inch diameter cavity with lucite walls. A 120° arc of conductive "dag" graphite was painted on the inside surface of the cavity to obtain a nearly radial electrostatic field in the vicinity of the collecting electrode. Platinum wire, 0.001 inch in diameter, located along the axis of the counter served as the collecting electrode.

The electric field distribution produced within the spherical cavity deviates from that obtained with a cylindrical geometry.

However, calculations have indicated that the error in the measured Y spectra will be less than 10 percent.

Calibration of the LET sensor was obtained with a 0.1 microcurie Am^{241} source mounted on a probe that could be positioned at various distances from the center of the sensitive volume. With the source at the surface of the cavity, uniform sensitivity of the cavity can be confirmed by measuring the distribution of pulse amplitudes from the counter with a multichannel analyzer. If the distribution is essentially rectangular (see Figure 6), sensitivity is constant throughout the proportional counter volume. With the source one centimeter from the surface of the cavity and the gas pressure constant at 0.25 atmosphere, the distribution presented by Figure 7 was obtained. Although the alpha particles at this distance from the source are not absolutely monoenergetic, their LET values are essentially constant within the sensitive volume of the counter; and a very narrow calibration peak was thus obtained. This peak was used to calibrate the system.

To accurately determine the energy deposited in the cavity by alpha particles originating at the calibration point, a Bragg curve for the Am^{241} was constructed by plotting multichannel analyzer relative channel number versus source position. The results of this experiment are presented in Figure 8. The area under the curve was set equal to 5.48 Mev, the energy of alpha from Am^{241}, and values for the ordinate were obtained. The intercept of the extrapolated curve in this case is 70 Kev/mm, whereas published experimental data for alpha particles in air corrected to methane give 65 Kev/mm, a difference of 7.8 percent, which is within the experimental error.

The sensitive volume of this unit was smaller than had been reported previously for proportional counters of this type. Advantages of using a small cavity include the following: (a) small sphere diameters can be simulated with reasonably high gas pressures; (b) Y spectra can be obtained in high intensity radiation fields; and, (c) the presence of the sensor provides a minimum disturbance to the uninstrumented radiation field.

The chamber designed for measurements of LET spectra at various depths in a tissue equivalent material for unidirectional beams with low penetrating power is shown in Figure 9. The sensitive volume of this counter is a 0.50 inch diameter cylinder with lucite walls. A 0.001 inch platinum wire is placed along the axis of the cylinder as an anode. The electric field distribution with this geometry is nearly ideal (a radial field inversely proportional to the radial distance from the anode) and columnar recombination is minimized for particles which traverse the cavity parallel to the anode. A 0.015 inch diameter collimator was used to define the point at which the LET spectra were obtained as well as the path traversed in the cavity by the incident particles. Calibration for this counter was identical to that used for the spherical counter except for the directional sensitivity evaluation.

Figure 10 illustrates the methane flow system that was used to adjust gas pressure in the cavity and maintain gas purity. A manostat was used to keep the gas in the cavity at a constant pressure and a needle valve was used to control the gas flow rate. By varying the methane pressure in the cavity, the equivalent unit density sphere size (or track length) could be varied over a wide range. In this experiment, simulated unit density dimensions were restricted to the range of 2.3 to 6.8 microns. This compares with an average yeast cell diameter of approximately 4.5 microns.

To determine if the gas flow was required to maintain satisfactory proportional counter operation, the counter was sealed at a pressure of 380 mm Hg. Calibration spectra were then obtained for a number of days and the results are presented in Figure 11. In this series of laboratory experiments, these data were not required since the methane pressure had to be continuously variable over a wide range. However, if instruments of this type are used in space experiments, it may be more economical to use a number of chambers sealed at different pressures than to construct a miniaturized gas flow and regulation system. In this case, it would be necessary to determine the long term stability of the instrument. If the gain does not drop below a predetermined value, slight changes in gain may not be important

if the system is continuously calibrated. This could easily be accomplished by permanently mounting a small Am^{241} source in the wall of the counter.

D. Phantom for 22.3 Mev Proton Experiments

The tissue equivalent phantom pictured in Figures 12 and 13 was constructed from lucite and filled with water. The instrument mounting bracket on top of the phantom could be positioned in a series of holes spaced one inch apart along the lucite. To obtain fine positioning control, a servo driven micrometer was used to position the instruments with an accuracy of $\pm$ 3 microns. An 0.015 inch thick lucite entrance window in the phantom was covered by a solenoid actuated shutter which completely stopped the 22.5 Mev proton beam. The shutter was used to accurately time control radiation exposure of the yeast cells and also to check background characteristics of the radiation measuring instruments.

E. Phantom for 210 Mev Proton Experiments

This tissue equivalent phantom was constructed from a solid lucite block and mounted behind a copper plate of sufficient thickness to stop 250 Mev protons. A remotely controlled solenoid actuated a shutter system which was used to check background radiation levels and control the exposure of the biological system. Ingots of yeast were held in place in the phantom by the arrangement illustrated in Figure 14. Numerous lucite blocks of different thicknesses were used to position the instruments at various depths.

III. EXPERIMENTAL RESULTS

A. X-Ray Irradiation

The x-ray source used to establish a reference point for the RBE determinations in this experiment was a Westinghouse 200 KVCP x-ray generator filtered with 1/2 mm Cu and 1 mm Al. With these filters the beam had a half value layer of 1.29 mm Cu and dose rates up to 8000 r per hour could be obtained at a distance of 12 inches from the target of the x-ray tube. For each exposure, the dose rates were measured with a Victoreen 100 r ionization chamber. In addition, the depth dose distribution in a tissue equivalent scattering medium (water phantom) was measured with a calibrated parallel plate ionization chamber. The results of these measurements are presented in Figure 15, along with the percentage of surviving yeast cells as a function of depth. No buildup of absorbed dose rate was observed near the surface of the phantom because of the relatively thick windows of the ionization chamber and water phantom.

The biological x-ray work was divided into two phases. During the first phase, the feasibility of the chosen biological system was studied and Figure 15 is presented as being typical of the results obtained after completion of the developmental phase of the biological system. Although the results of sectioning only one ingot are presented, it should be pointed out that in a duplicate ingot, irradiated after the first ingot was removed, the results varied by no more than 10 percent at any given depth.

Feasibility studies were conducted to determine the possibility that ionizing radiation may depolymerize the polyethylene glycol and result in toxicity to the cells over and above the damage caused cells by ionizing radiation. Accordingly, polyethylene glycol was irradiated with x-rays up to total doses of 300 k rad, and immediately added to yeast cell suspensions. No resultant toxicity was observed for x-rays, and later, proton irradiation also failed to give detectable toxicity. The suspending medium was, therefore, adjudged bland and nontoxic to yeast cells.

Phase two of the x-ray studies established the baseline for RBE determinations. Figure 1 illustrates the type of killing curve obtained with yeast cells suspended in polyethylene glycol after irradiation with 200 KVCP x-rays. Because there is a radio protective effect due to dehydration after suspensions of yeast cells are placed in polyethylene glycol, a killing curve with wet yeast cells is presented on the same graph for comparison.

B. 22.3 Mev Proton Irradiation

The first series of proton irradiations was performed with the 86 inch cyclotron at the Oak Ridge National Laboratory. This accelerator can produce a reasonably uniform beam of 22.3 Mev protons which have a range in lucite of approximately 0.4 centimeters. Tissue absorbed dose rates from approximately one to over 10^6 rad per hour could be obtained a few inches from the beam exit port. This wide dynamic range permitted a rapid exposure of the biological systems at high intensities and accurate LET spectra measurements at relatively low intensities.

To determine the exact position of the beam, a zinc oxide film was positioned a few inches in front of the beam exit port. When the proton beam was on, this film produced a glow defining the cross-sectional area and location of the beam which was observed and recorded with a remote television monitoring system. The phantom was then clamped in position so that the instruments and biological systems would be located at the geometrical center of the beam.

Figure 16 illustrates the sample holder and position arrangement used for irradiating the biological systems. Before striking the yeast ingot, the beam traversed a short air path, the 375 micron thick entrance window on the water phantom, and the thin foils used on the transmission chamber. The beam then penetrated about 4000 microns into the yeast ingots which were of sufficient length to completely stop the protons. With this arrangement, the unirradiated portion of the ingot nearest the

sample holder could be used as a control. An advantage of using this technique is that biological killing data were obtained for numerous LET spectra and rad doses simultaneously. The total absorbed dose received by the biological system was controlled by the calibrated transmission chamber and a remotely activated solenoid. First, the transmission chamber was calibrated with a tissue equivalent ionization chamber to determine the radiation absorbed dose rate at a depth of 1140 microns in the compacted mass of yeast cells for various ionization currents. An Elcore current integrator was then used to determine the absorbed dose by integrating the current over the exposure time for each ingot.

To determine the depth dose distribution in the water phantom, a tissue equivalent ionization chamber was placed at 100 micron increments along the path of the proton beam. The ratio of the ionization current produced in this chamber to that produced in the transmission monitoring chamber was then determined as a function of depth in the water phantom. These results are presented in Figure 17.

LET spectra were measured at various depths in the water phantom using both the cylindrical and spherical proportional counters. However, because the beam intensity was high and reasonably unstable, only the results obtained with the cylindrical counter were used. The cylindrical counter also permitted a more exact determination of the depth at which a specific LET spectra was obtained. This was due to the fact that the protons in the collimated beam had to traverse varying thicknesses of tissue equivalent material before entering the spherically shaped cavity.

LET spectra measured at various positions in the phantom with a simulated track length of 2.3 microns are presented in Figures 18 through 22. Each curve has been normalized to correspond to an absorbed dose of one rad.

For three of these LET spectra, Y spectra have been calculated and are presented in Figures 23 through 25. In this experiment, the average values of Y differ from

the average values of LET by a constant. Thus, any correlation that is obtained between LET and biological effectiveness can also be obtained for average Y. This would not be the case if the directional properties of the radiation environment were unknown.

The effects of increasing the simulated track length to 4.5 and 6.8 microns are shown in Figures 26 through 32. Inverse logarithmic slopes of the biological killing curves and average LET values are presented in Figure 33 and Table IV.

As expected, the curve in Figure 33 representing a simulated track length of 2.3 microns corresponds to significantly higher values of average LET than those for longer track lengths. The average LET values taken from this graph were selected for the primary correlation of the biological and physical data.

As a first approximation, it has been assumed that over a limited range, the curve relating RBE to LET is a straight line on a semilog plot. This assumption is in agreement with data that have previously been reported in the literature. Thus, the product of the inverse logarithmic biological killing slope times average LET should remain constant at various depths in the phantom. Table IV compares these products at five different depths. It is interesting to note that the most constant value of this product is obtained for a simulated track length of 4.5 microns, the average diameter of the yeast cells when embedded in polyethylene glycol.

Results obtained after irradiating the yeast ingots with 22 Mev protons produced clear cut biological expressions of the Bragg peak which occurred when the proton beam was stopped in the tissue simulant. Figure 34 is a plot of a family of curves showing per cent of yeast cell survivors versus depth with total dose at 1140 microns as the parameter. Bragg peak killing is evident for each experiment and extends through a depth of 600 microns. In general, all samples showed a decreasing killing effect from the surface to about 1500 microns where a plateau was reached

Depth in Phantom (Microns)	Inverse Killing Curve Slope	Average LET kev/micron			Normalized Product of Inverse Killing Curve Slope And Average LET		
		2.3*	4.5	6.8	2.3	4.5	6.8
3130	48.2	23.5	8.5	3.8	100.0	100	100.0
3480	45.0	29.5	9.5	4.5	117.0	104	112.0
3680	40.1	36.5	11.0	5.5	129	108	121
3780	34.9	41.5	12.0	6.0	128	102	115
3880	28.8	48.0	13.0	7.0	122	91	111

* Beginning numbers of each column represent simulated track.

TABLE IV: Comparison of Inverse Killing Curve Slope with Average LET.

which continued to about 3000 microns depth at which point the Bragg peak began. Peak killing was reached at a depth of about 3800 microns. The survivors rose sharply to equal the unirradiated controls at a depth of about 4200 microns.

The greater killing consistently observed at the surface of the ingots was probably due to two factors: greater oxygen tension[14,18]; and secondary radiations generated by the protons penetrating the metal foil monitoring device which is part of the cyclotron. Work with x-rays under an atmosphere of nitrogen and subsequent work with 210 Mev protons proved that the effect of oxygen diffusing into the first few hundred microns of the ingot accounted for most of the increased killing, and little was due to soft radiation. Curve 1 in Figure 17 is a plot of proton dose as a function of depth within the water phantom and Curve 2 is a plot of yeast cell per cent survivors.

An interesting phenomenon occured at the low dose of 1200 rads. The plateau is at the 100 percent survivors level for several hundred microns. Similar results were found with 210 Mev protons at an incident dose of 1440 rad.

C. 210 Mev Proton Irradiation

The 130 inch synchro-cyclotron at the University of Rochester was used for this series of experiments. This machine produces a reasonably uniform 210 Mev proton beam that can penetrate approximately 28 cm of tissue equivalent material. Dose rates from this machine can be varied from nearly zero to approximately 400 rad per hour. Relative intensity measurements of the beam profile had been previously measured with a scintillation counter which had a small lucite head that was movable horizontally and vertically.[12] The results of these measurements are presented in Figure 35.

To insure proper alignment of the beam, photographic images of the beam were obtained at two locations along the beam path. An optical alignment system was then used to move the phantom into position.

The extra penetrating power of the 210 Mev protons as compared with the 22 Mev protons necessitated a redesign of the phantom and a rearrangement of the biological system. The phantom was machined from lucite with a long cylindrical hole to hold 7 ingots placed end to end. (See Figure 14). Since it is necessary to mount an ingot on a microtome holder prior to irradiation in order to assure accuracy of dimensions in sectioning, lucite microtome holders were made for each ingot. The holding rod was fitted into the holder by threads. The rod was removed prior to irradiation and the resulting hole was filled with polyethylene glycol to assure approximate tissue equivalency throughout the entire length of the proton path through the series of ingots.

To determine the depth dose distribution in the lucite phantom, a tissue equivalent ionization chamber was placed at several positions along the path of the beam. As in previous experiments, the ratio of the ionization current produced in this chamber to that produced in the transmission monitoring chamber was determined as a function of depth in the phantom. These results are presented in Figure 36. The peak of the ionization curve occured at 24.8 cm. Secondaries produced in the air and transmission chamber probably account for the relatively high surface dose.

Since the dose rates produced by the machine were very low, most of the available machine time was used to irradiate the biological system. It was, therefore, impossible to measure the Y spectra for this portion of the experiment.

For the radiation studies with the biological system, a series of ingots were prepared in the usual manner with Sc-7 yeast. The ingots were carefully chosen to assume uniformity of bore size, yeast density, and paraffin density. Since the final chosen ingots came from several batches, it was necessary to have an unirradiated control ingot from each batch.

The linear dimension of each ingot and its holder was carefully measured with a vernier caliper. The ingots were then placed in sequence in the bore of the phantom and flown to Rochester, New York, for irradiation.

The unirradiated controls were also sent in order to insure more comparable conditions during the course of the experiment and the inherent time delays.

On the return to the laboratory, each ingot was carefully sectioned at pre-planned intervals. At each interval, three 100 micron slices were taken. Each slice was diluted and plated in quintuplicate. Each point on Figure 36 thus represents the average of three samples taken within a 300 micron interval and involving 15 petri plates.

The increased killing at the beginning of each ingot was due to the previously described oxygen effect as well as to soft radiations. An oxygen effect was found at the beginning of each ingot except number 3. (No oxygen effect was found at the end of the ingots because they were well sealed to the lucite holders.)

The absence of the oxygen effect at the beginning of ingot 3 is regarded as additional evidence that no killing occured in this area of the ingot. It should also be noted that no detectable killing of the yeast cells was found from 7 through 12 cm of depth in the ingots.

Detectable killing began at 13 cm in ingot 3. Unfortunately, the Bragg peak began in the lucite holder of ingot 5 and at the beginning of ingot 6. Due to the oxygen effect, the first interval sampled in ingot 6 gave more killing than is considered valid. Complete absorption of the beam occured by 32 cm (in ingot 7) and again no detectable effect was present.

IV. REVIEW OF OBJECTIVES AND GENERAL DISCUSSION

It is generally recognized that many experiments designed to study the correlation between LET and RBE have had certain shortcomings. Some of these shortcomings resulted from the inability to accurately measure the radiation absorbed dose. Thus, variations in RBE have frequently been masked by inadequate dosimetry. Adequate dosimetry presumes an accurately controlled irradiation geometry, for which depth dose distributions and local variations in radiation intensity can be measured or accounted for. This problem becomes acute when irradiating monolayers of cells.[13] Under these conditions, dose rates are usually calculated from the physical properties of the radiation field.

With the exception of few experiments, only average LET values have been correlated with RBE. However, the use of average LET values should be restricted to irradiation experiments for which there is very narrow spread of LET values. There are two reasons for this. First, to adequately evaluate the effects associated with delta rays, free radical diffusion, etc., a compacted mass of cells must be used instead of cell monolayers. The second reason for this is illustrated in Figure 37. The curve relating RBE to LET can be established by irradiating a thin biological specimen with a monoenergetic beam of various types of particles that lose only a small amount of their kinetic energy in passing through the specimen. By way of contrast, the two LET spectra illustrated by curves a and b could have the same average LET values but differ significantly in their biological effectiveness in a given experiment. It is, therefore, necessary when evaluating the quality of an unknown radiation field in the laboratory[7] or in space, to obtain a complete measurement of the distribution of dose in Y or LET. To eliminate some of the problems normally associated with these investigations, and at the same time, develop an instrument for measuring the quality of ionizing space radiations, the following objectives were established for this research program.

1. Refine currently available spaceflight instrumentation which will measure the absorbed dose at a point within a scattering medium.

2. Develop spaceflight instrumentation which will measure the linear energy transfer (LET) spectra at a point within a scattering medium.

3. Show the relationship between the viability of yeast cells and absorbed dose at essentially the same point within a scattering medium.

4. Show the relationship between the viability of yeast cells and LET spectra with absorbed dose held constant and at essentially the same point within a scattering medium.

For the reasons outlined in the introduction, the second objective was modified to include the development of a Y sensor. The requirement for constant dose was eliminated because the RBE for haploid Saccharomyces cerevisiae used for these experiments in independent of dose.[19] Aside from these two modifications, the original objectives of this research program have been completed.

The biological system developed for this research program has yielded reproducible and heretofore unavailable data on the killing effects of protons and x-rays. In addition, the complete experimental system (biological and instrument systems) is sensitive enough to detect slight differences in RBE.

As a result of this experimental program, it is now possible to measure directly the distribution of dose in LET (or Y) produced by high energy particle accelerators. This work was based in part on concepts originally proposed by Rossi, and used primarily for evaluating D(Y) spectra resulting from neutron irradiation. With slight modification of the instruments, this technique can be extended to measurements of unknown radiation environment.

V. RECOMMENDATIONS FOR FUTURE WORK

The success of this program in evaluating the relationship between radiation quality and relative biological effectiveness indicates that the instrument systems and biological techniques developed could be very useful for making more detailed studies of the mechanisms of radiation interactions with living matter. For example, cells other than yeast can be embedded with this technique and, indeed, may yield better results than those obtained to date. In this way, an accurate determination of the variation of RBE with LET spectra over a wide range of LET values could be determined.

The technique should also be used to determine the variation of biological response with the very high values of LET obtained from multiple charged heavy ions. Results of such experiments could be very useful in evaluating the radiation hazards associated with primary cosmic rays.

An evaluation of biological radiation damage other than the ability to form a macroscopic colony from a single cell should also be performed. For example, biological techniques described in this report would be very useful for determining the effect of LET on genetic mutations.

The extreme accuracy afforded by the microtome sectioning of the embedded cells would also make it possible to determine the three dimensional spread of radiation damage resulting from a radiation microbeam striking the ingot of cells at right angles with respect to the ingot length.

With only slight modifications, the radiation quality sensors developed for this program could be used to measure the distribution of dose in Y at various positions in a tissue equivalent phantom exposed to the space radiation environment. By comparing the data from such an experiment with the results obtained in the laboratory, the radiation hazards associated with manned spaceflight could be assessed.

As described in numerous articles by Rossi, instrumentation techniques described in this report are also applicable to neutron dosimetry problems.

In addition, this experimental system should be used for evaluation of the experimentally shown change in RBE when a biological system within a magnetic field is exposed to radiation.

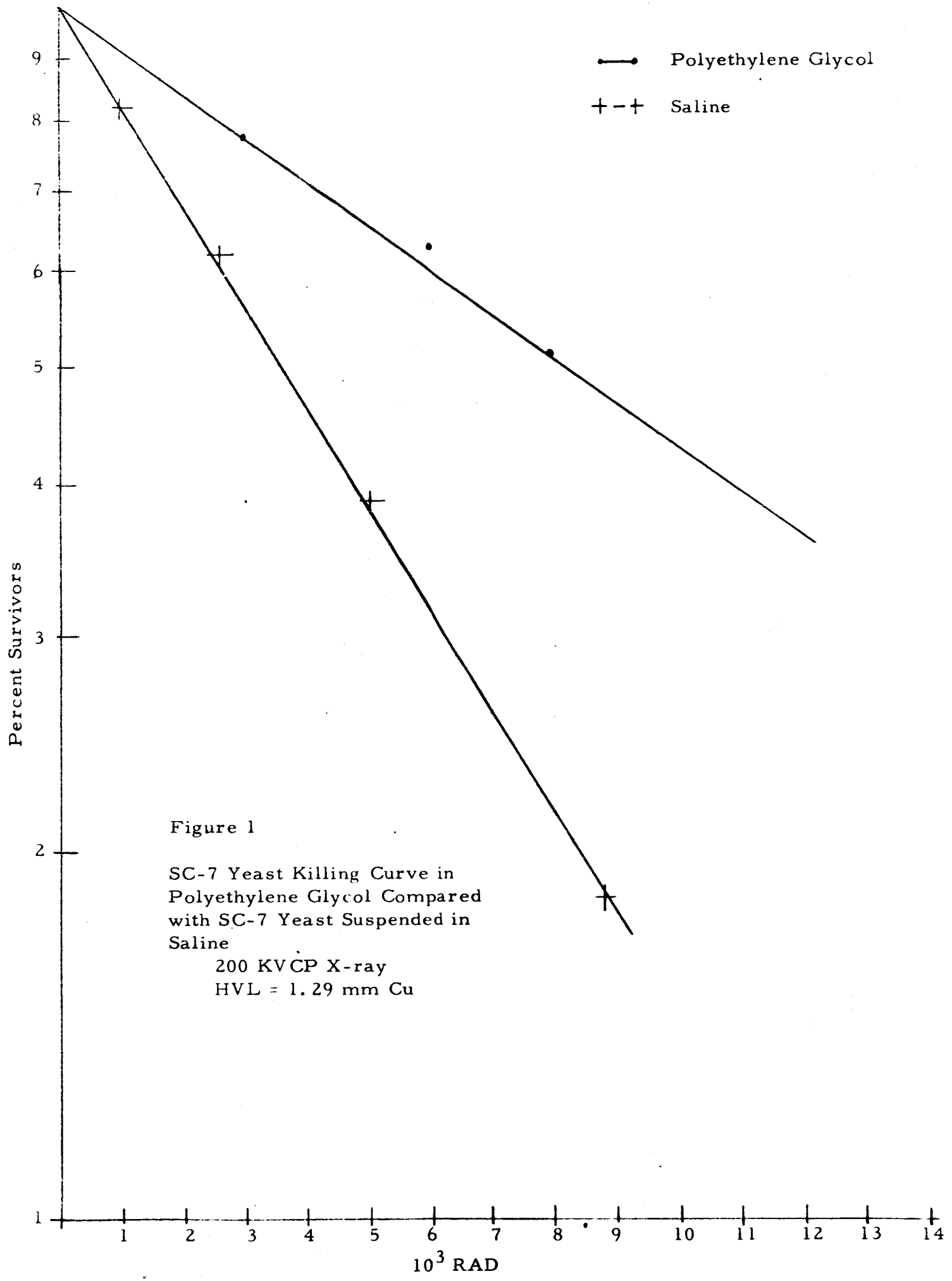

Figure 1

SC-7 Yeast Killing Curve in Polyethylene Glycol Compared with SC-7 Yeast Suspended in Saline

200 KVCP X-ray
HVL = 1.29 mm Cu

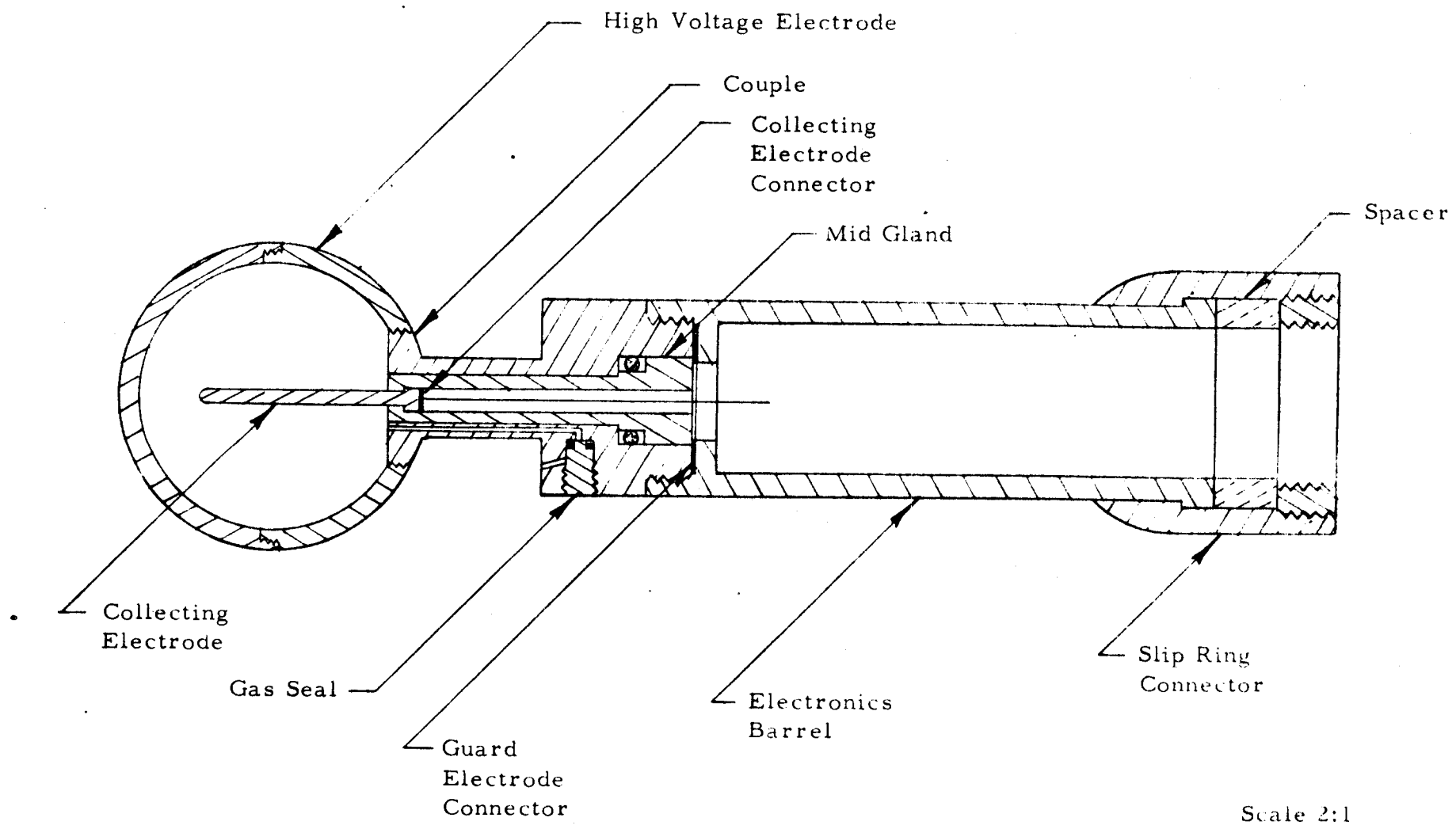

Figure 2. Basic Chamber Design

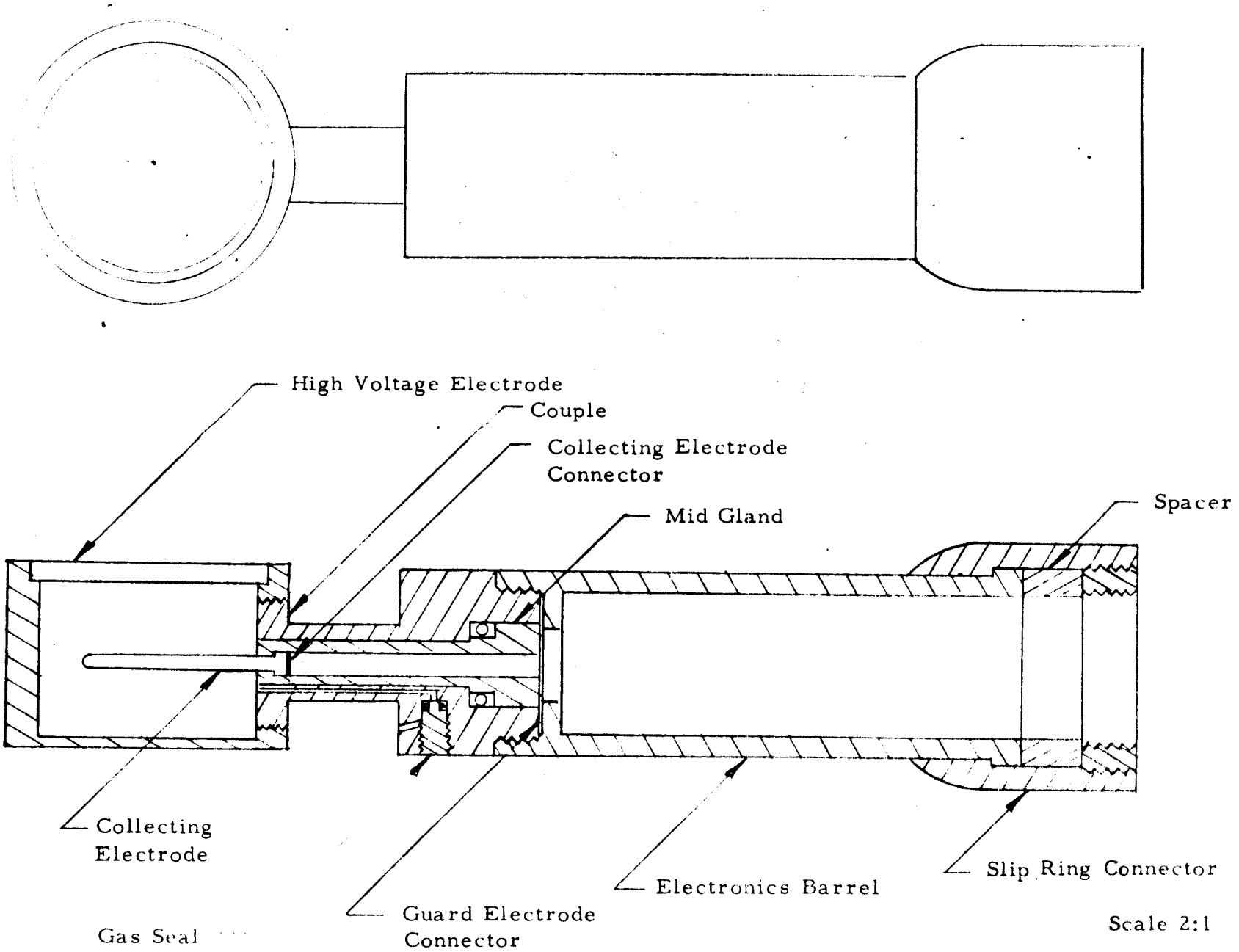

Figure 3. LET Ion Chamber

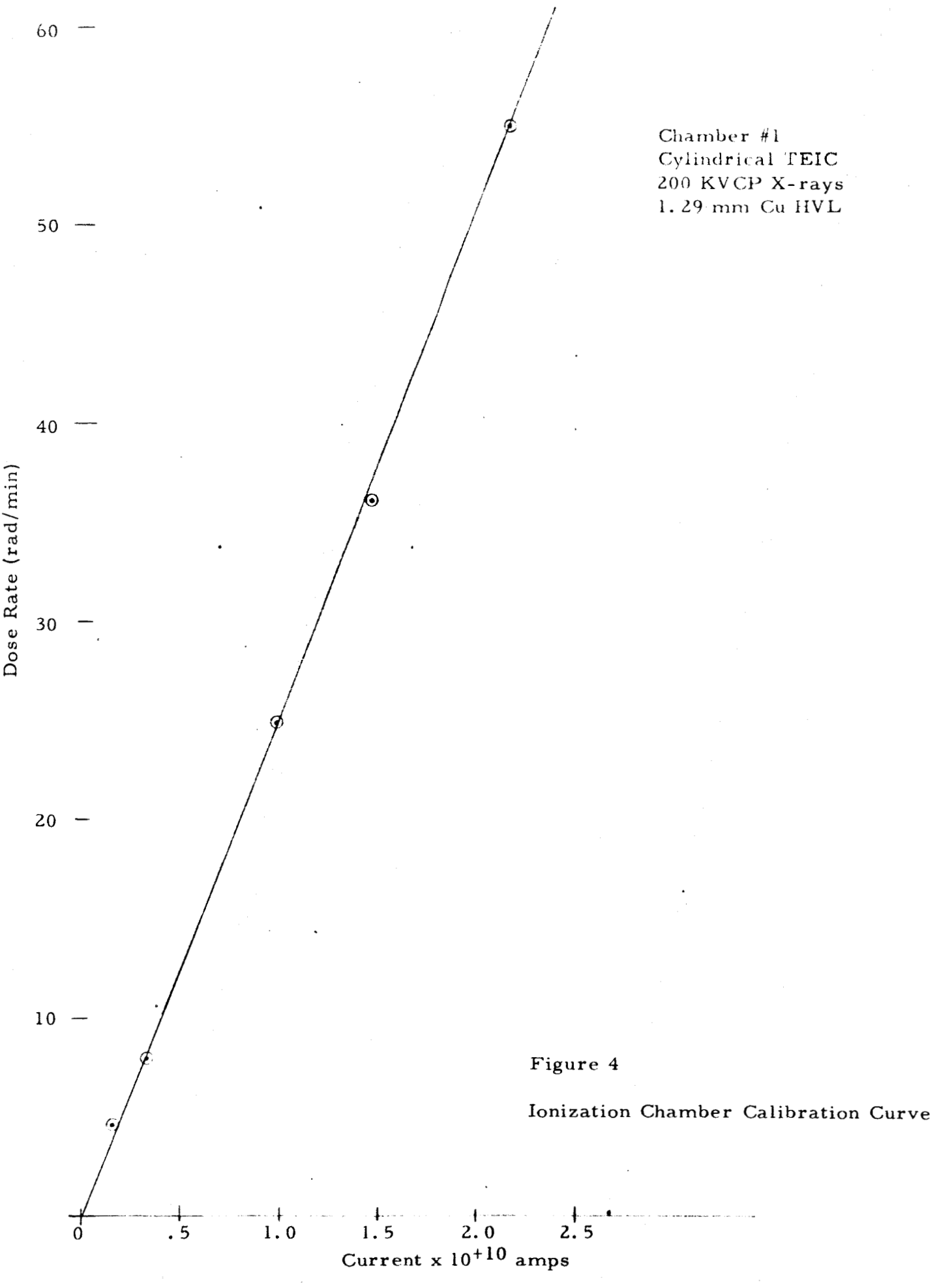

Figure 4

Ionization Chamber Calibration Curve

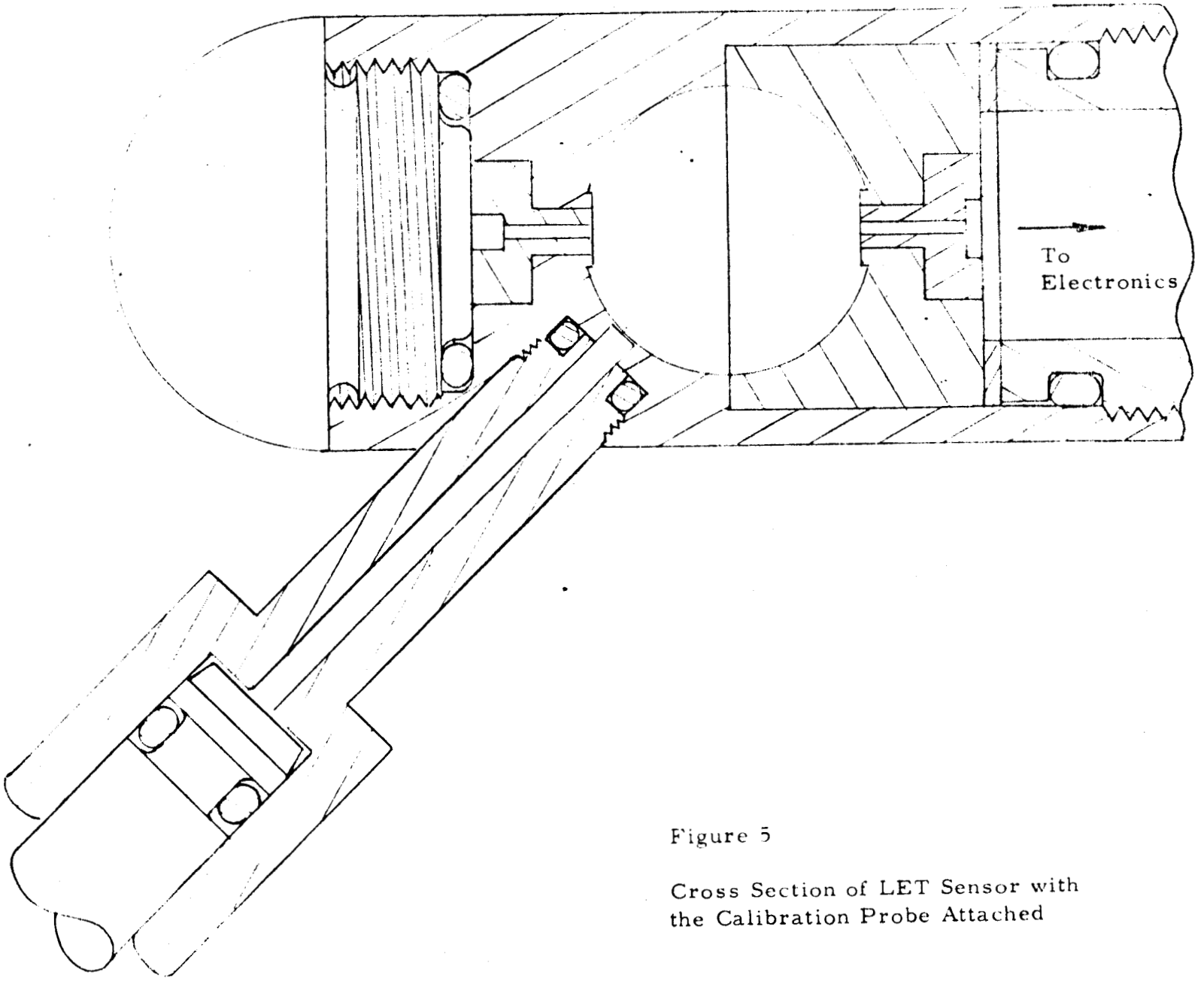

Figure 5

Cross Section of LET Sensor with
the Calibration Probe Attached

FIG. 6

AMERICIUM 241 PULSE HEIGHT DISTRIBUTION

1/2 ATMOSPHERE CH_4

AMERICIUM 241 AT SURFACE OF PROPORTIONAL CHAMBER

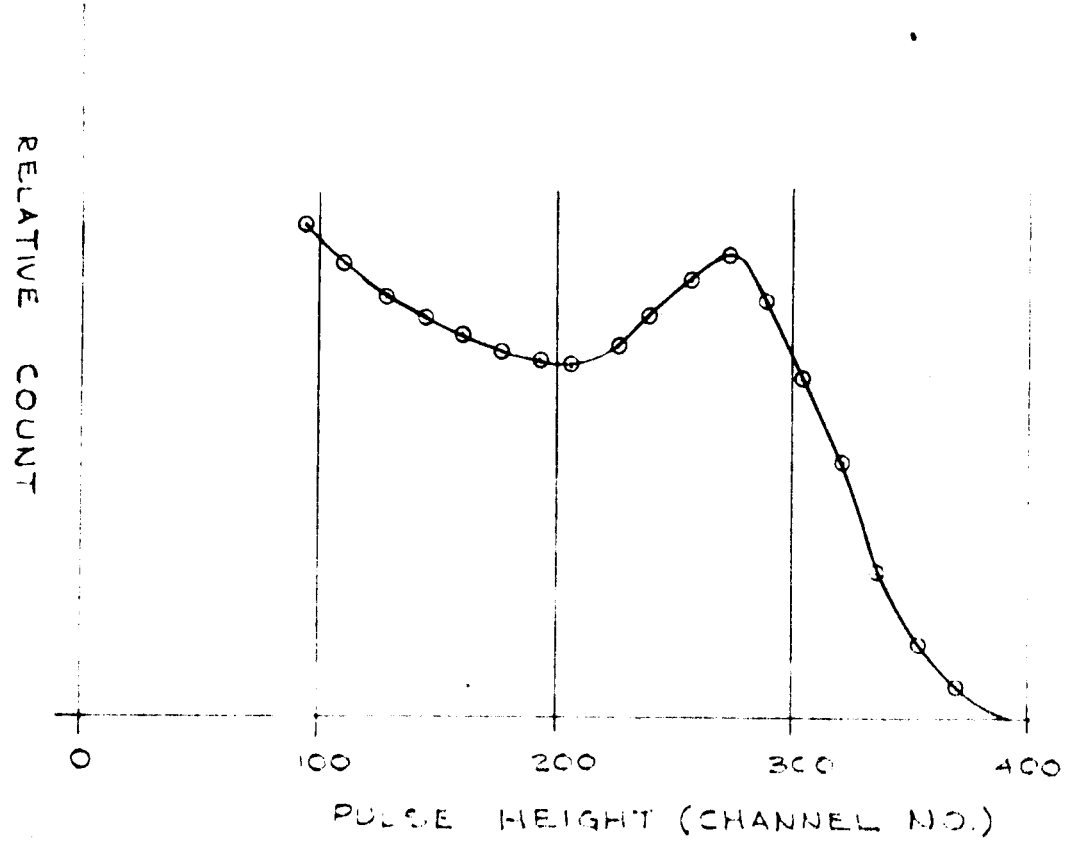

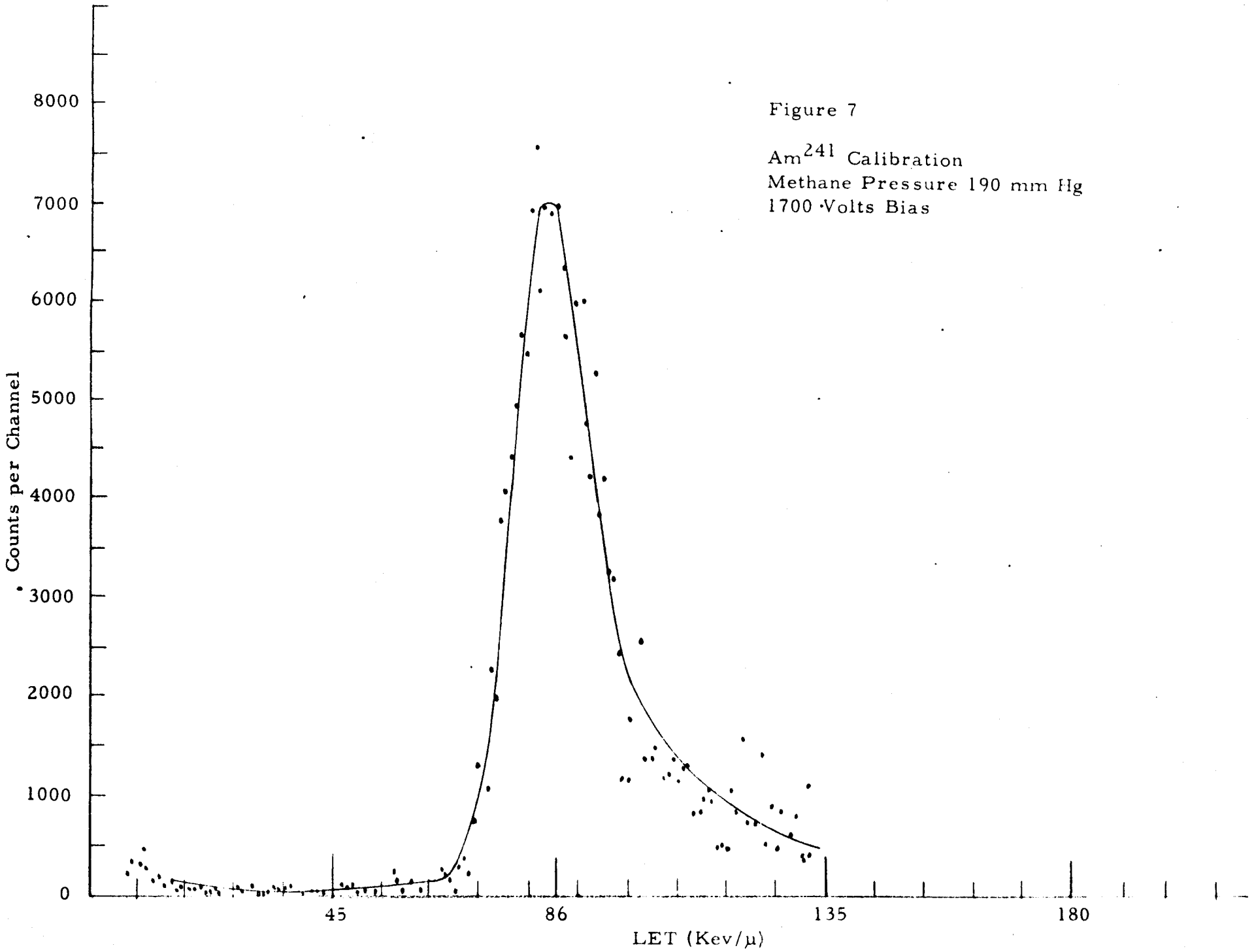

Figure 7

Am^{241} Calibration
Methane Pressure 190 mm Hg
1700 Volts Bias

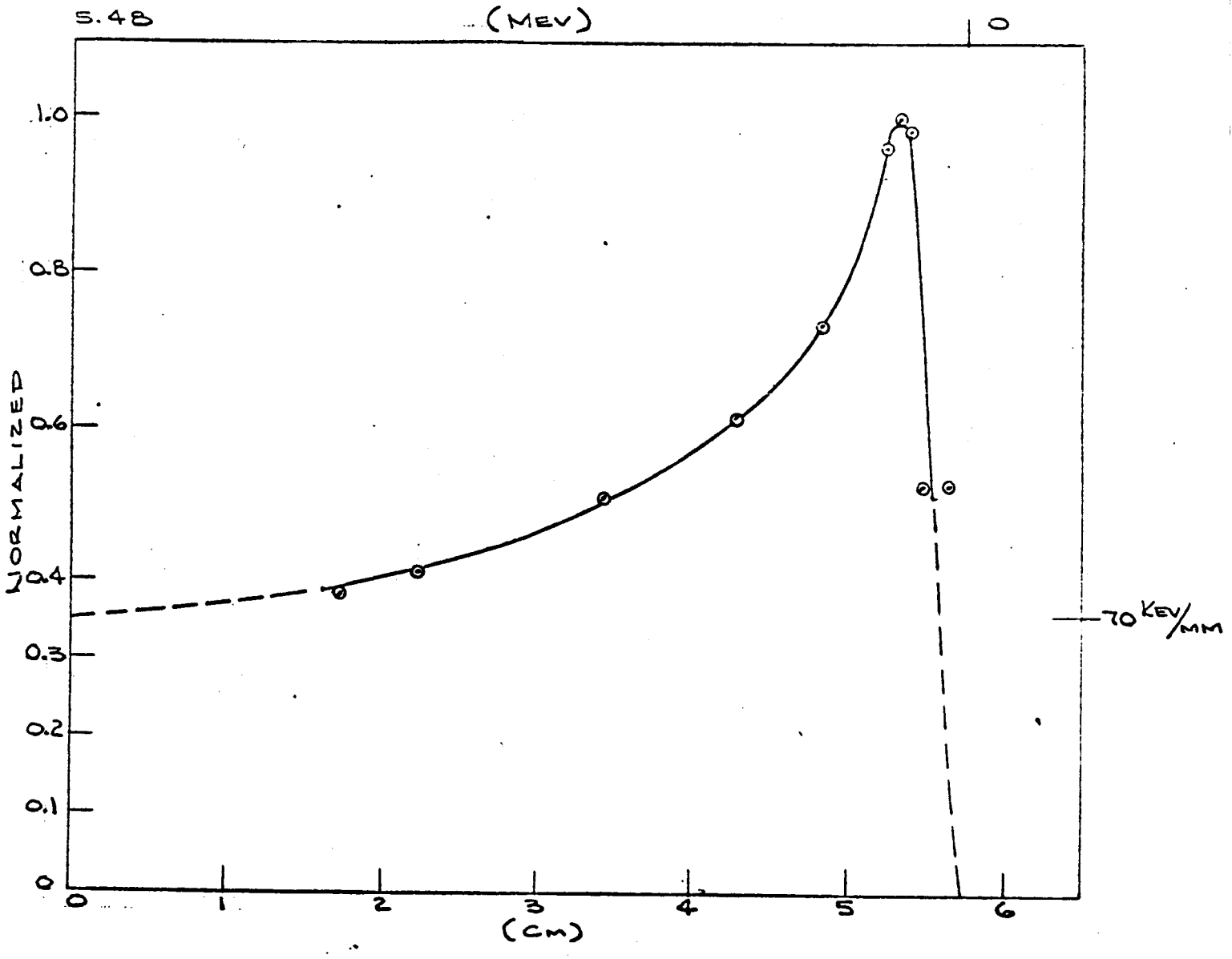

FIG 8
PLOT OF RELATIVE CHANNEL NUMBER VERSUS SOURCE DISTANCE

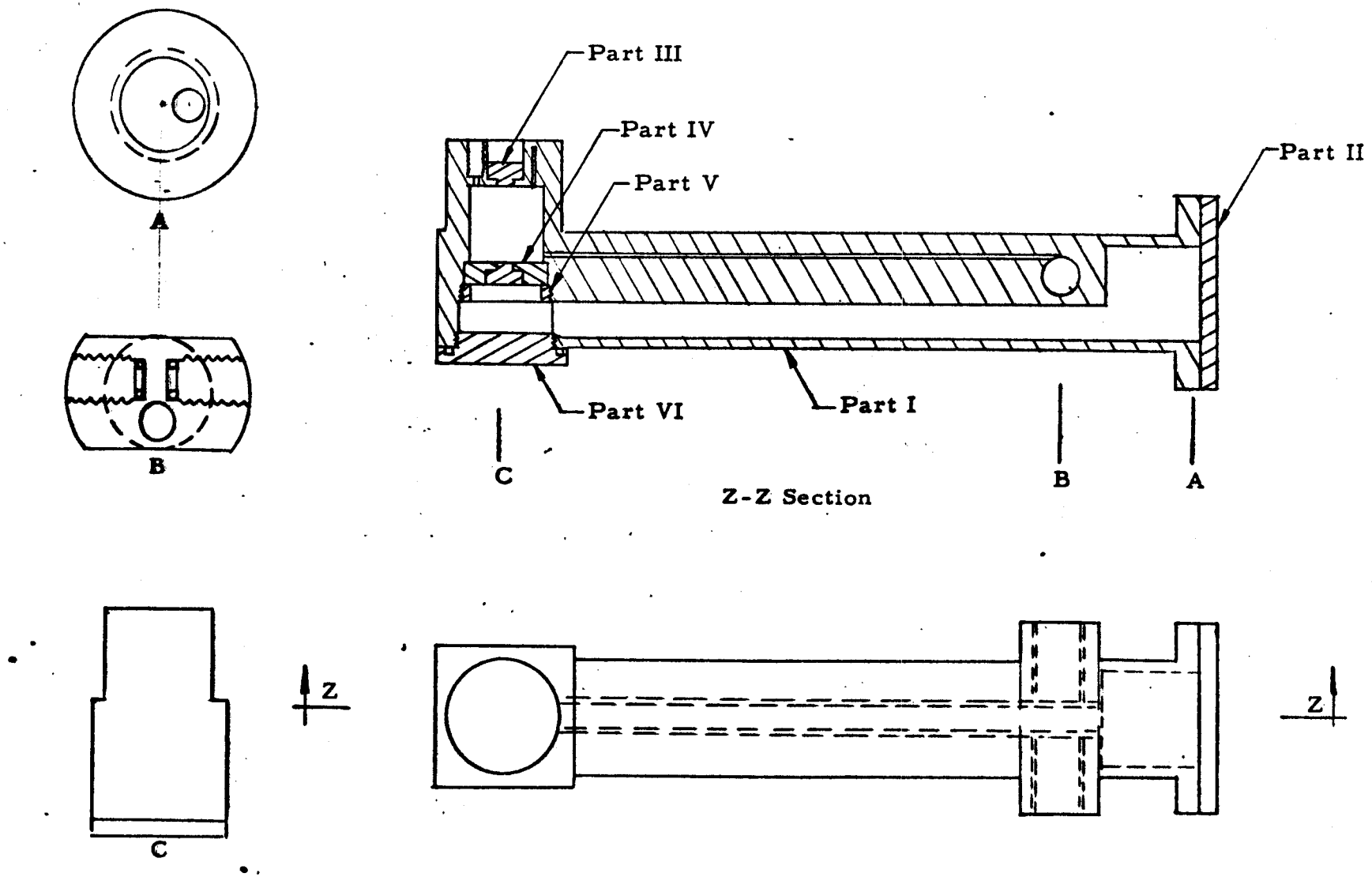

Figure 9

Cross Section of Cylindrical LET Sensor

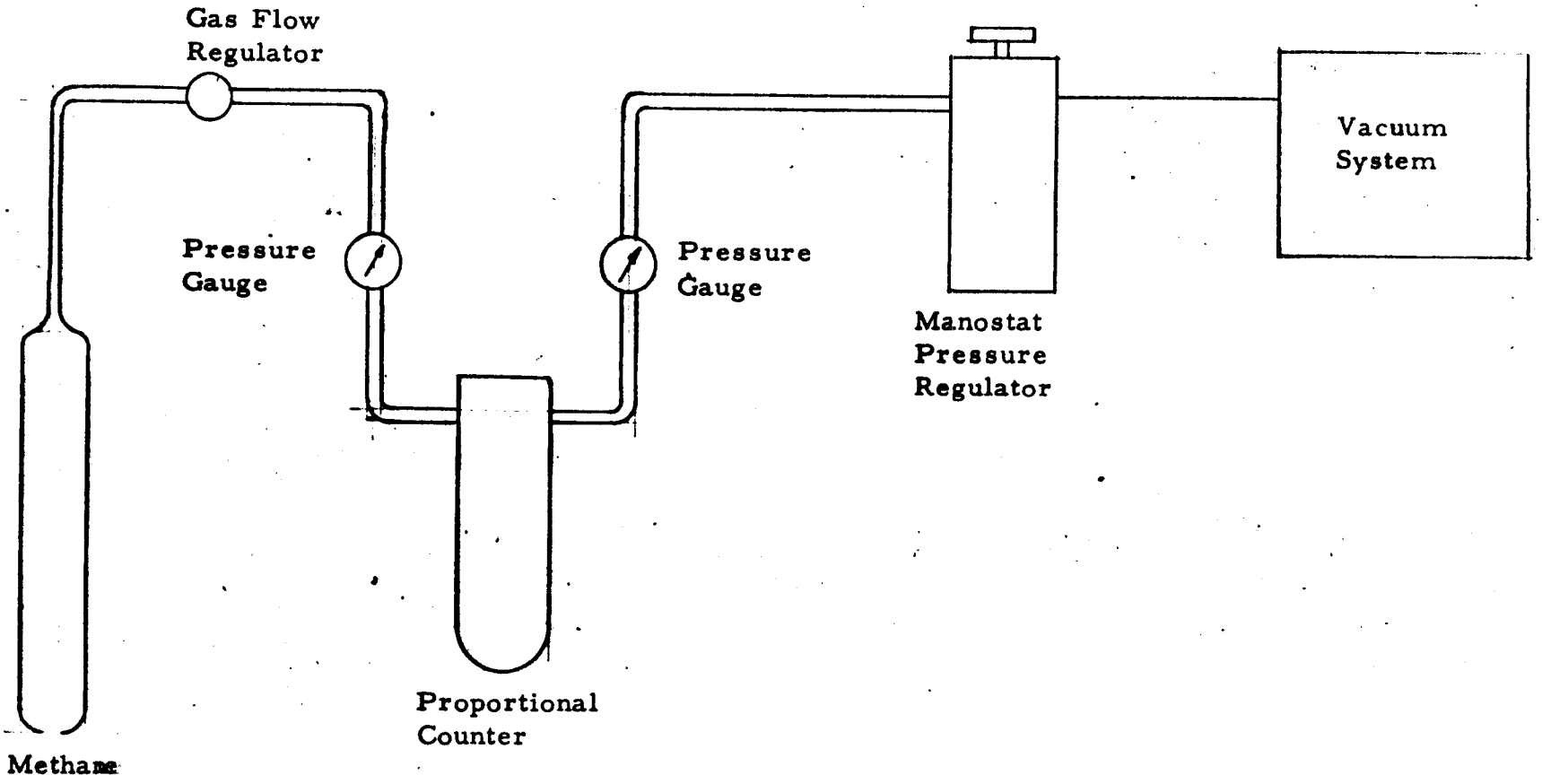

Figure 10 Gas Flow System

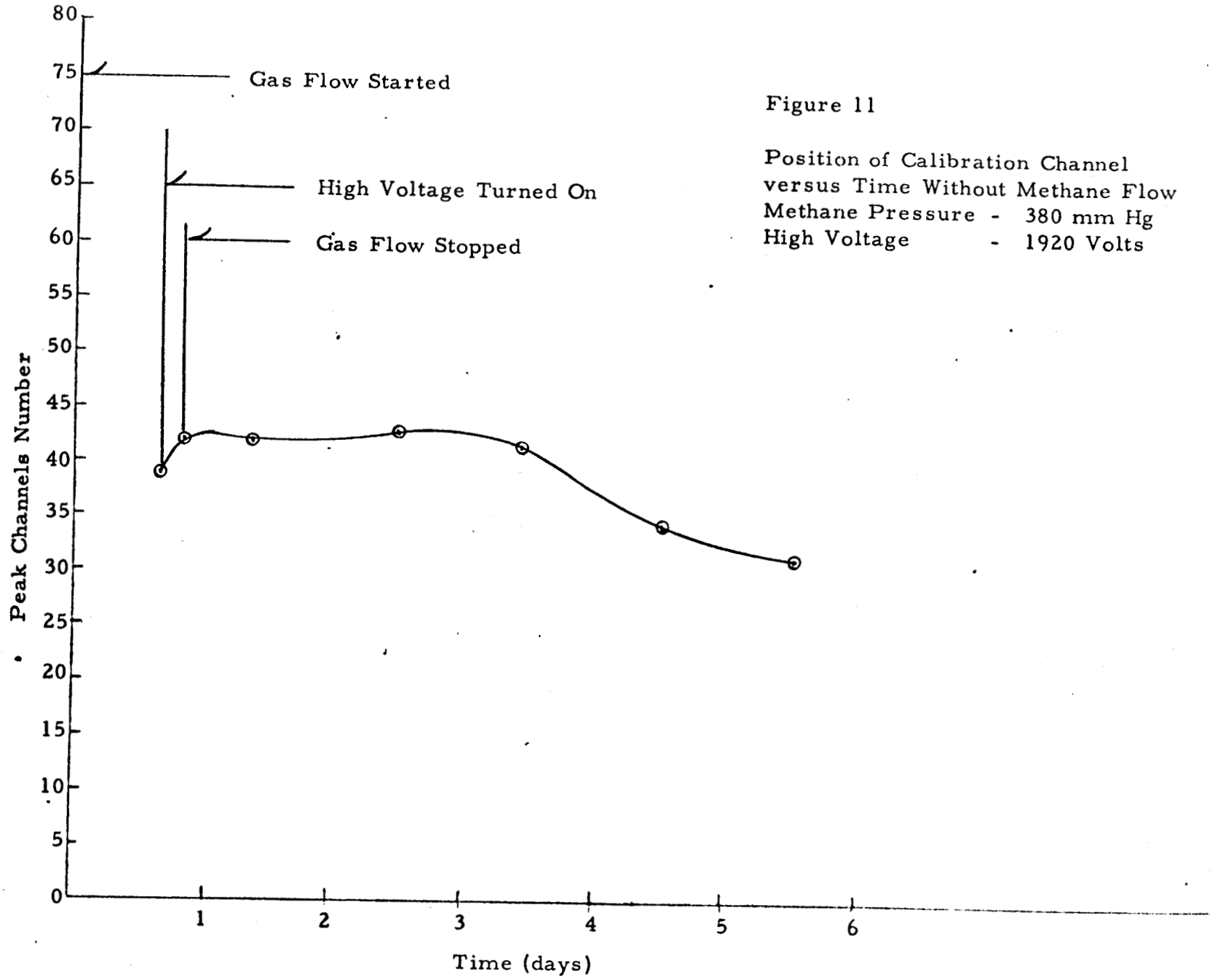

Figure 11

Position of Calibration Channel
versus Time Without Methane Flow
Methane Pressure - 380 mm Hg
High Voltage - 1920 Volts

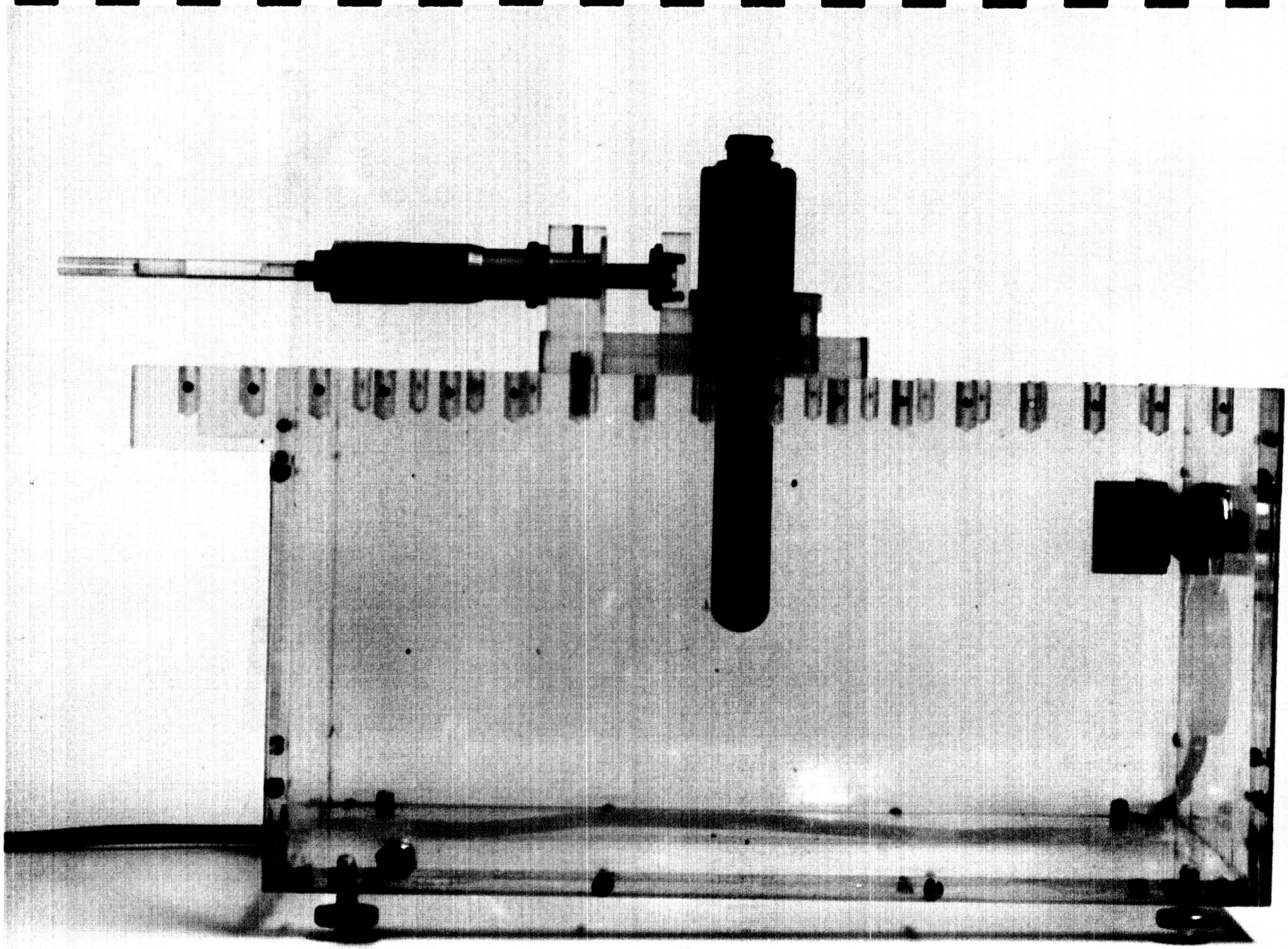

Figure 12

Side View of Water Phantom

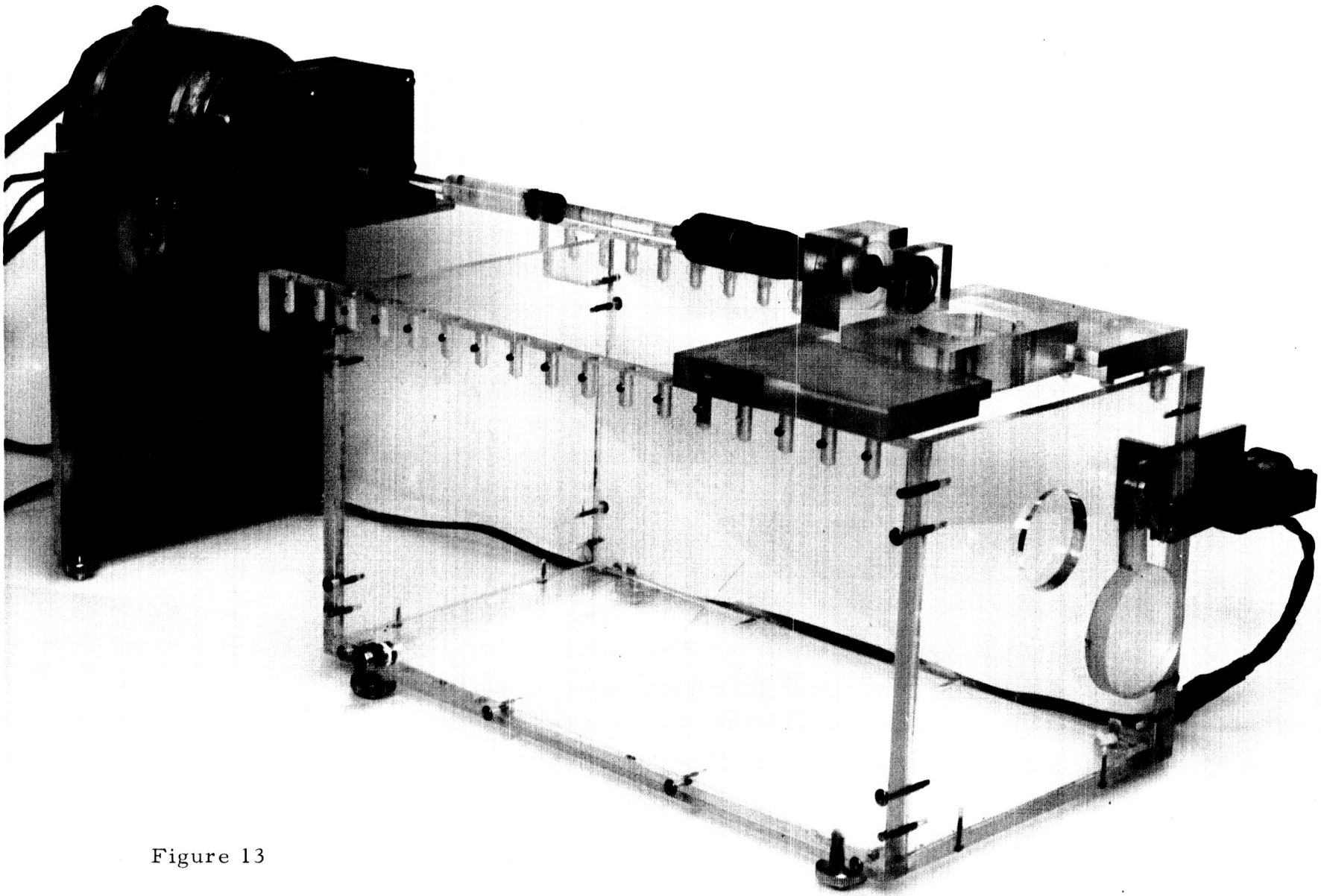

Figure 13

Water Phantom
Showing Servo Control

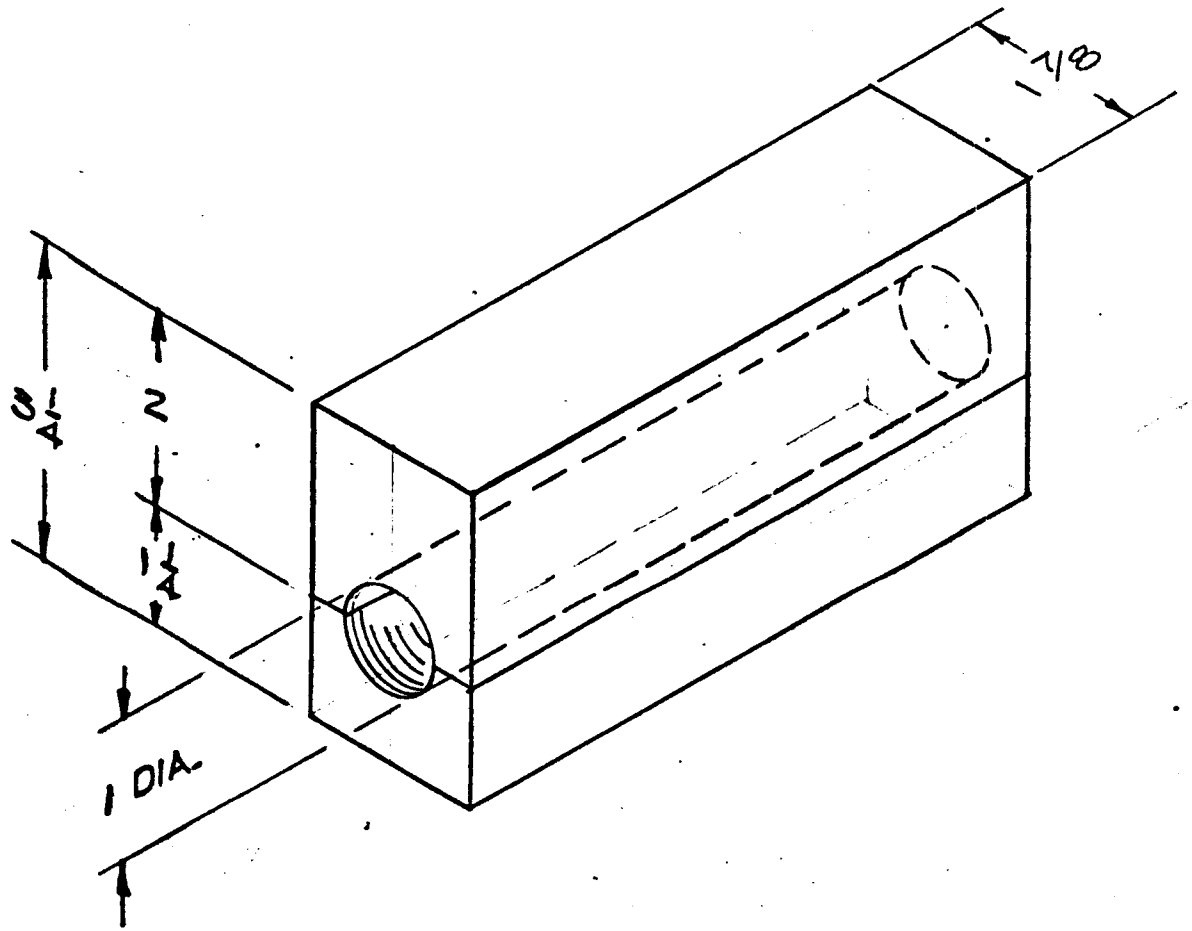

Figure 14

Arrangement for Holding Ingots in Lucite Phantom

Figure 15

Depth Dose and Killing Curves
for 200 KVCP X-rays
Filters - 0.5 mm Cu + 1.0 mm Al
HVL - 1.29 mm Cu

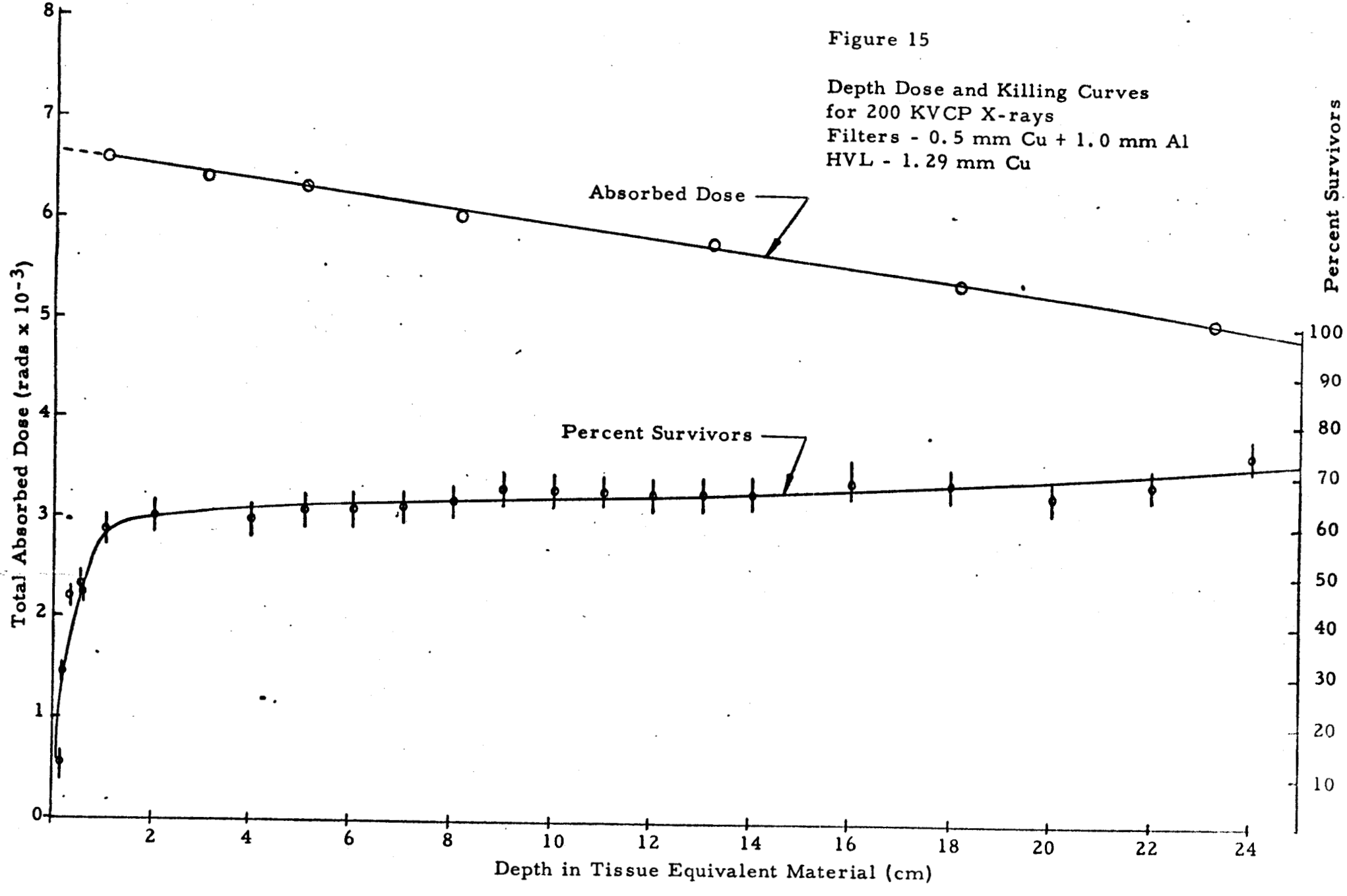

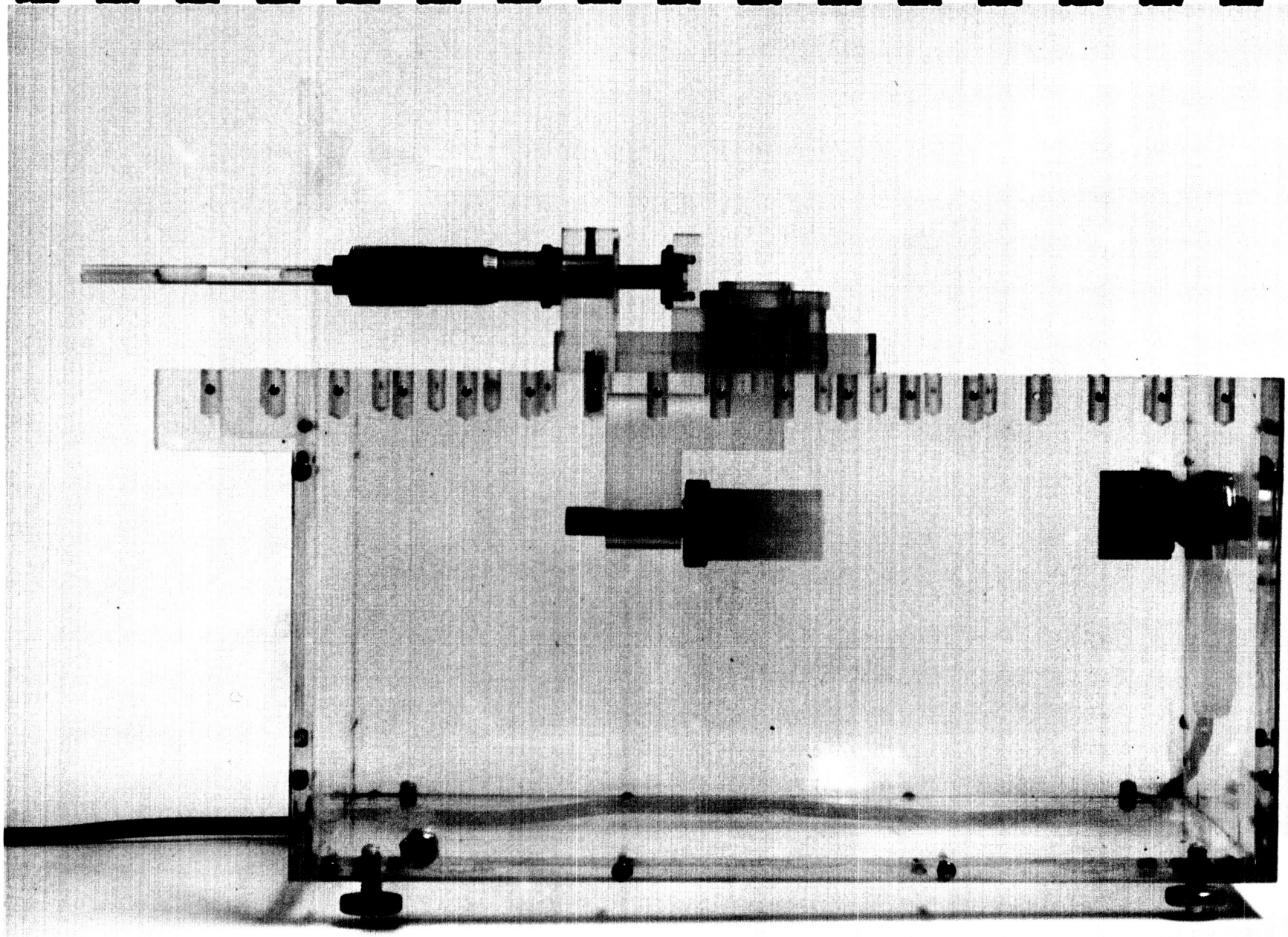

Figure 16

Photo of Yeast Ingot
Held in Water Phantom

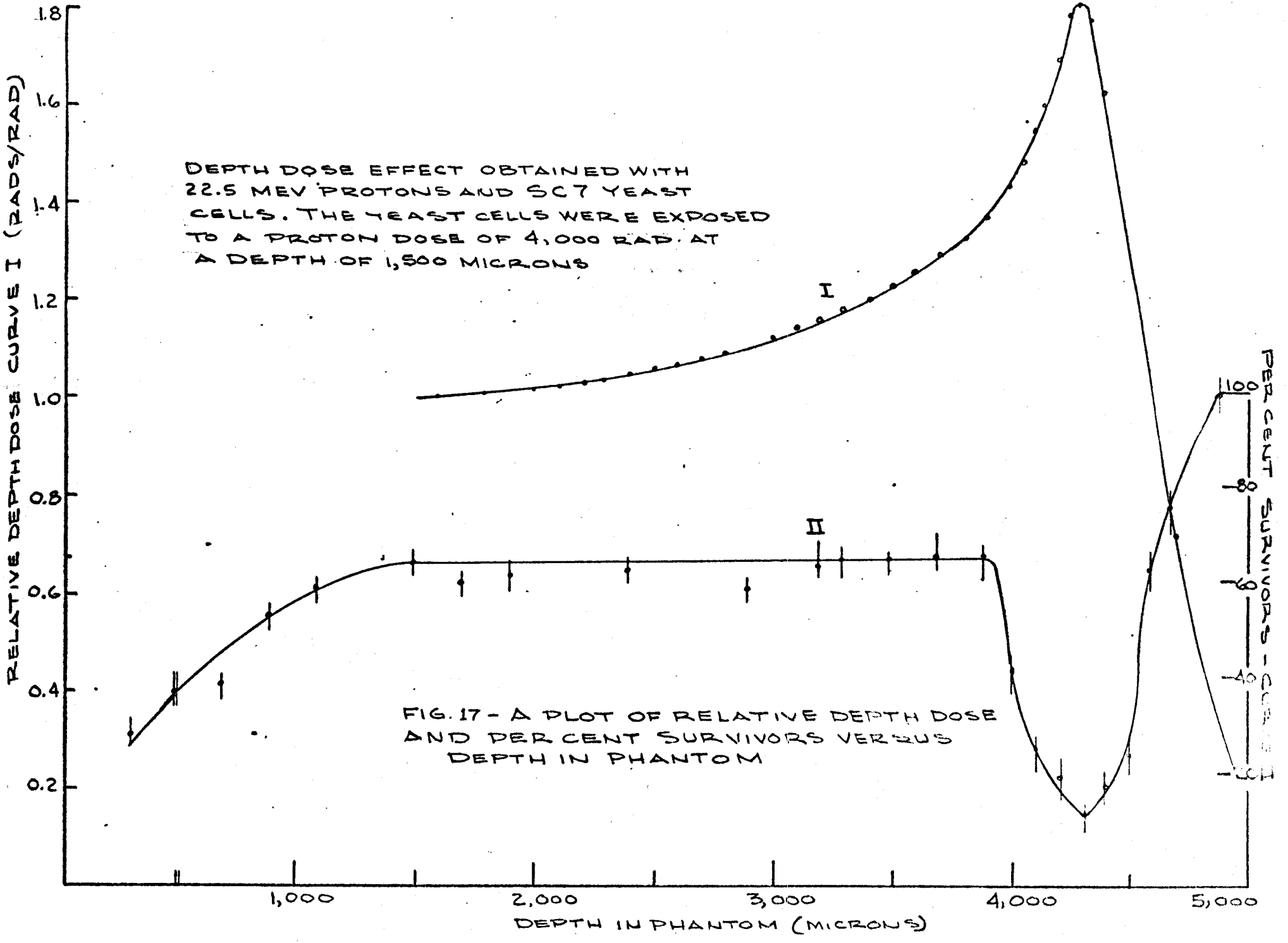

FIG. 17 - A PLOT OF RELATIVE DEPTH DOSE AND PER CENT SURVIVORS VERSUS DEPTH IN PHANTOM

Figure 18

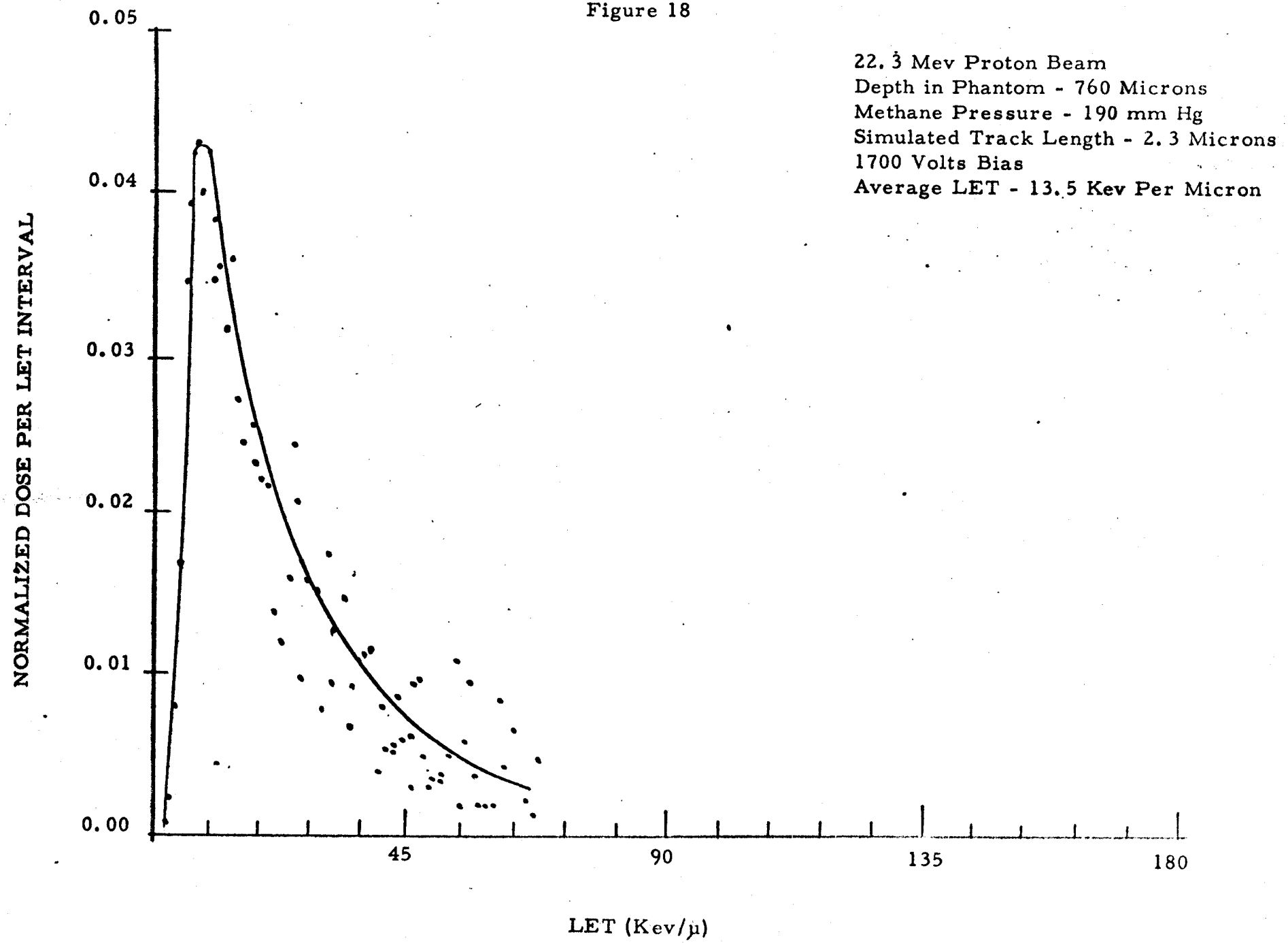
22.3 Mev Proton Beam
Depth in Phantom - 760 Microns
Methane Pressure - 190 mm Hg
Simulated Track Length - 2.3 Microns
1700 Volts Bias
Average LET - 13.5 Kev Per Micron
NORMALIZED DOSE PER LET INTERVAL
0.05
0.04
0.03
0.02
0.01
0.00
45
90
135
180
LET (Kev/μ)

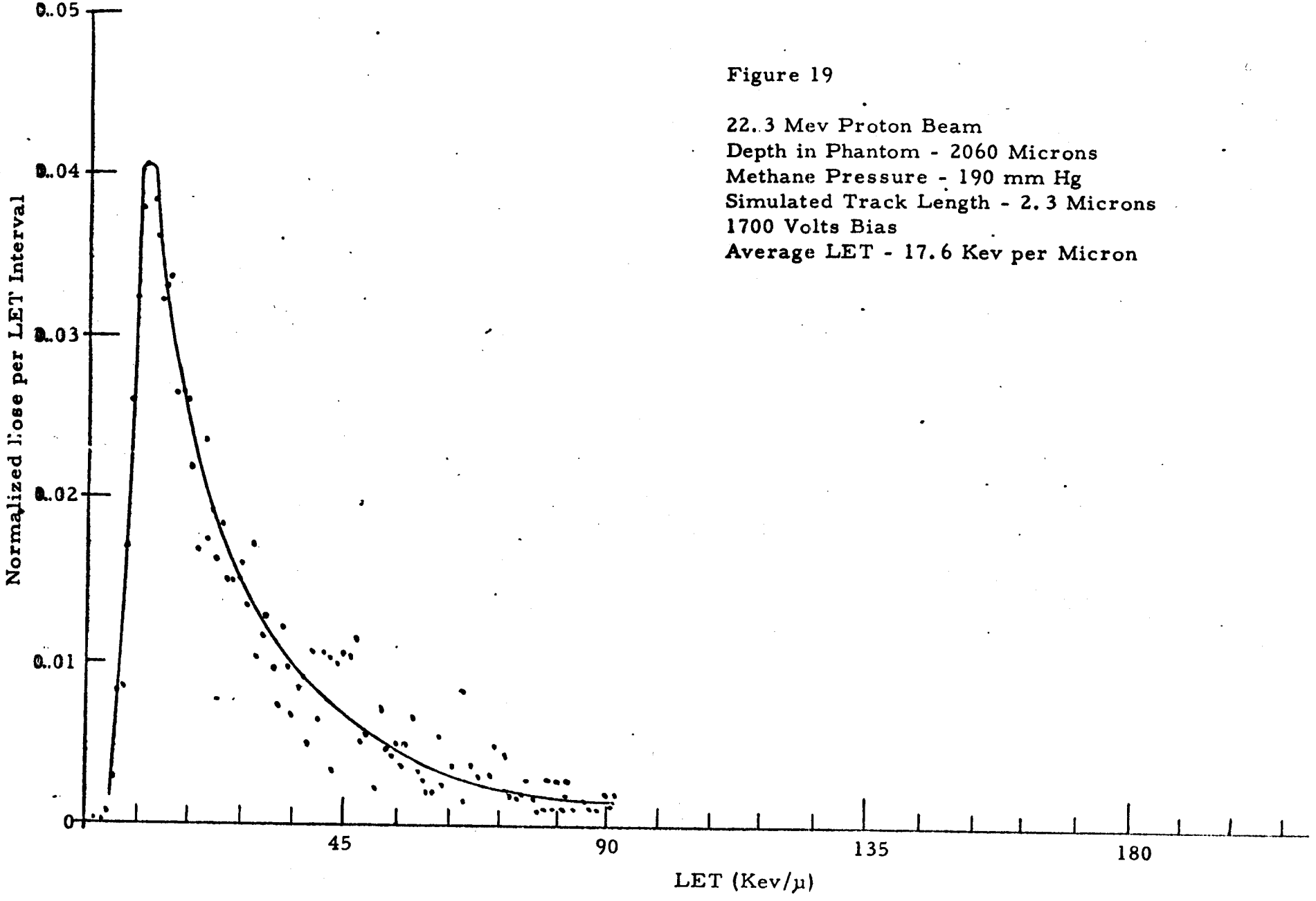

Figure 19

22.3 Mev Proton Beam
Depth in Phantom - 2060 Microns
Methane Pressure - 190 mm Hg
Simulated Track Length - 2.3 Microns
1700 Volts Bias
Average LET - 17.6 Kev per Micron

Figure 20

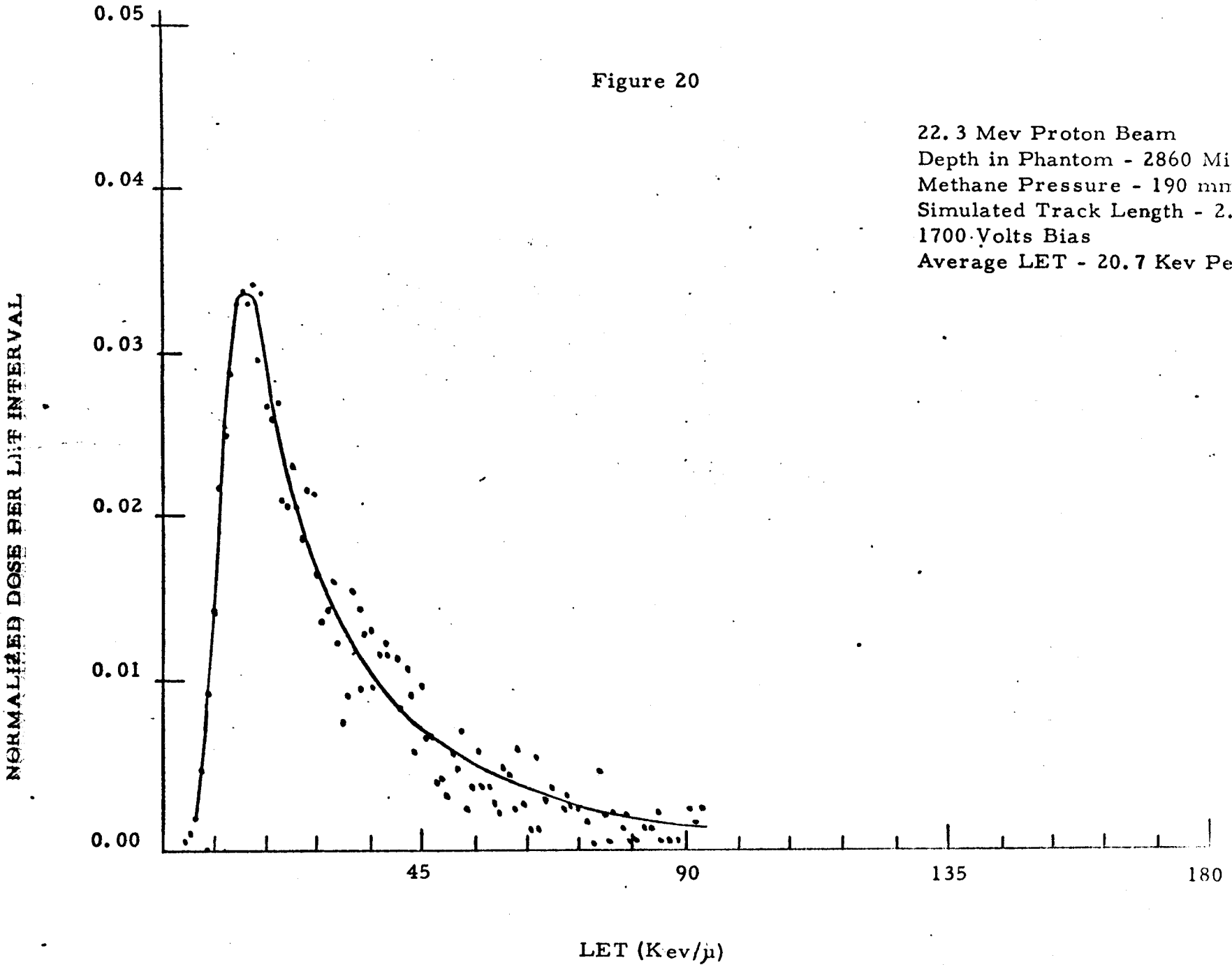
22.3 Mev Proton Beam
Depth in Phantom - 2860 Microns
Methane Pressure - 190 mm Hg
Simulated Track Length - 2.3 Microns
1700 Volts Bias
Average LET - 20.7 Kev Per Micron
NORMALIZED DOSE PER LET INTERVAL
0.05
0.04
0.03
0.02
0.01
0.00
45
90
135
180
LET (Kev/μ)

Figure 21

22.3 Mev Proton Beam
Depth in Phantom - 3660 Microns
Methane Pressure - 190 mm Hg
Simulated Track Length - 2.3 Microns
1700 Volts Bias
Average LET - 34.7 Kev Per Micron

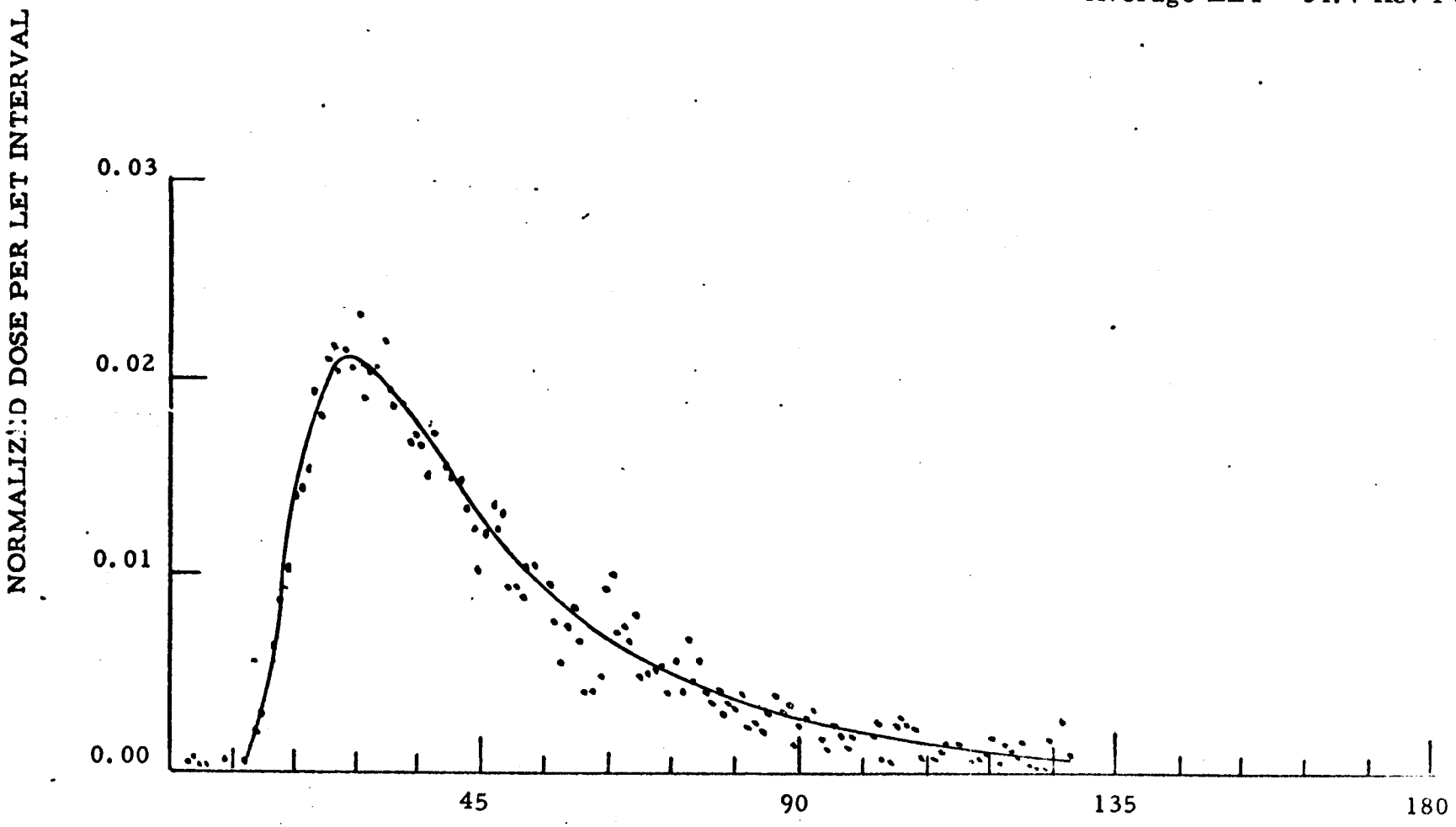

Figure 22

22.3 Mev Proton Beam
Depth in Phantom - 4060 Microns
Methane Pressure - 190 mm Hg
Simulated Track Lenth - 2.3 Microns
1700 Volts Bias
Average LET - 72.9 Kev Per Micron

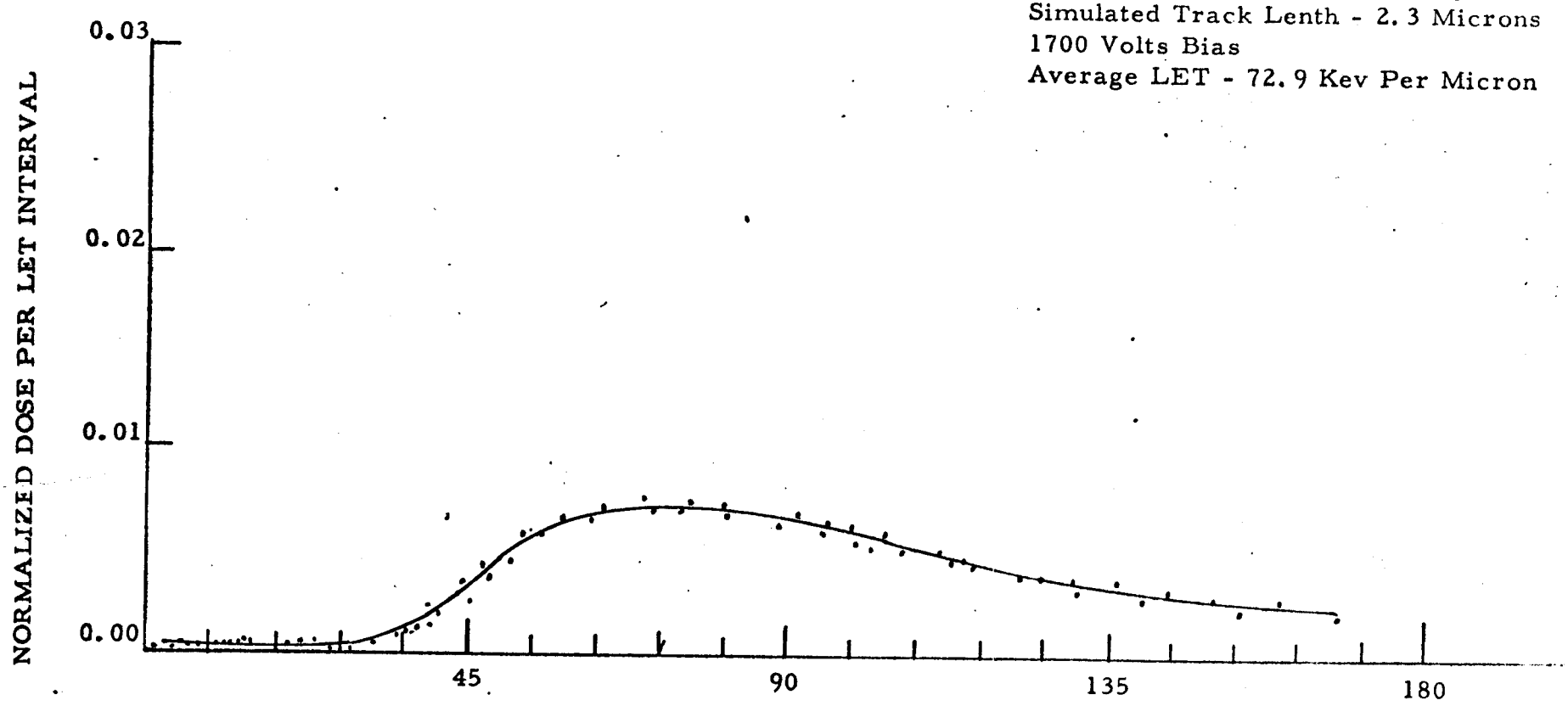

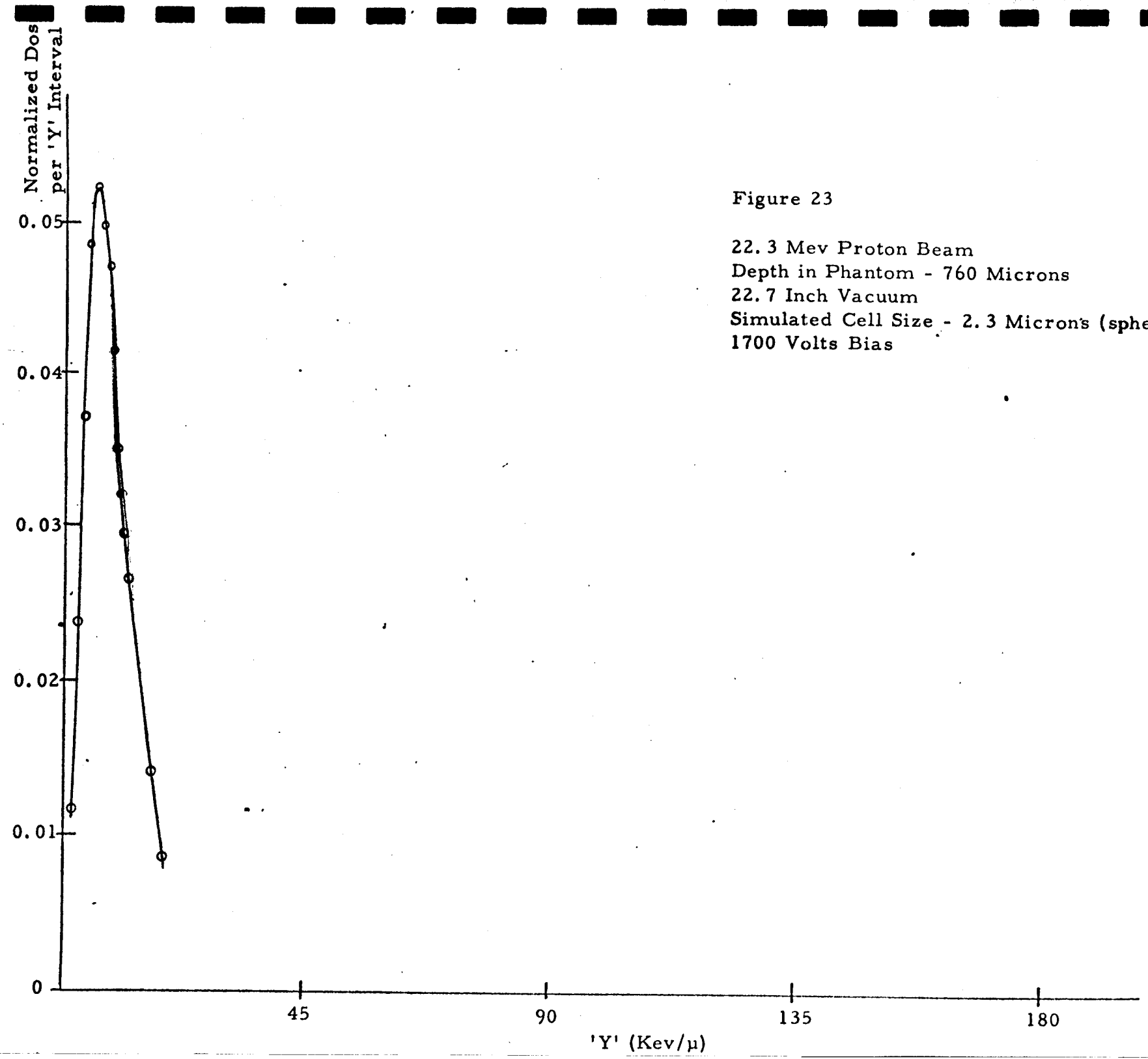

Figure 23

22.3 Mev Proton Beam
Depth in Phantom - 760 Microns
22.7 Inch Vacuum
Simulated Cell Size - 2.3 Micron's (spherical)
1700 Volts Bias

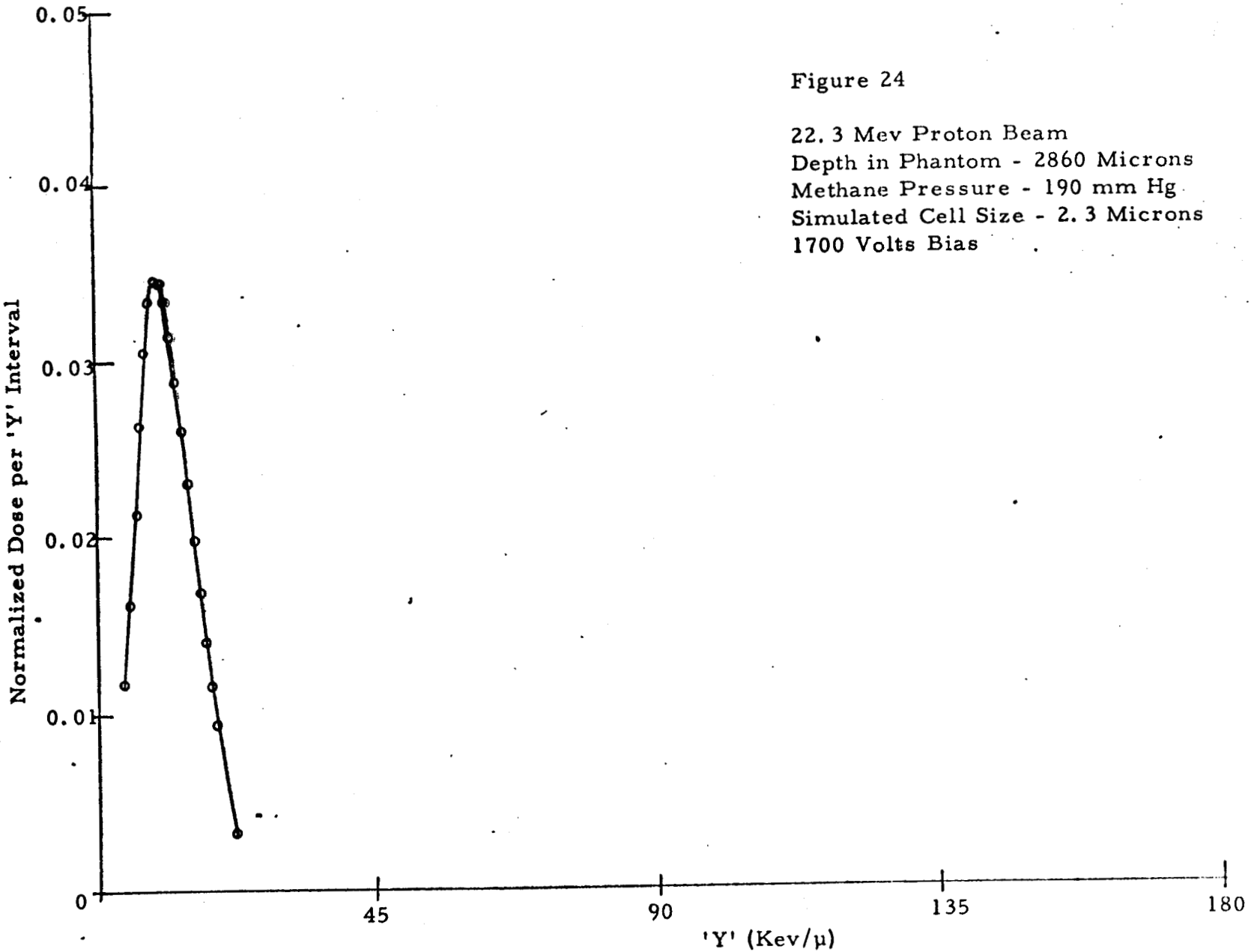

Figure 24

22.3 Mev Proton Beam
Depth in Phantom - 2860 Microns
Methane Pressure - 190 mm Hg
Simulated Cell Size - 2.3 Microns
1700 Volts Bias

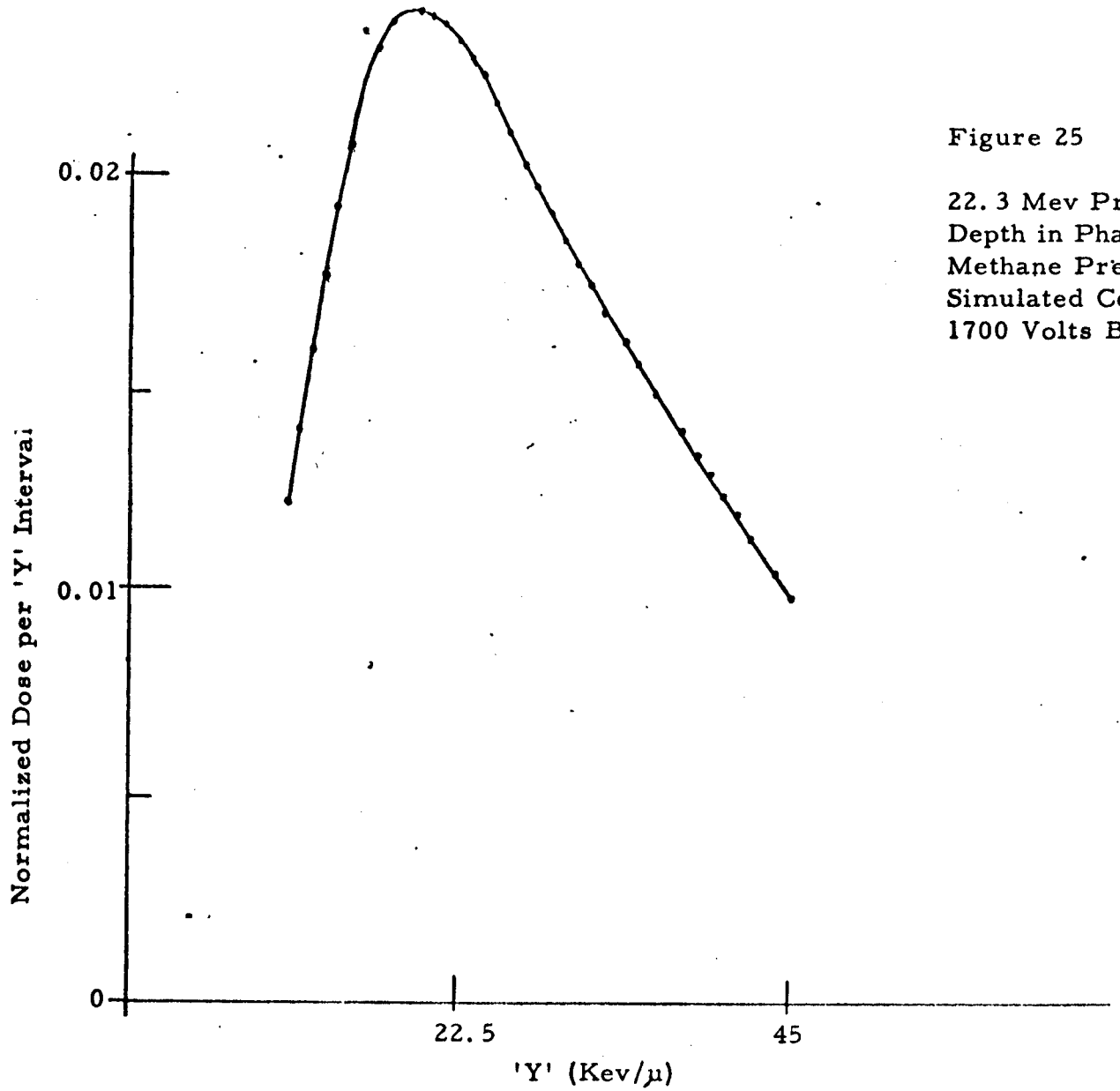

Figure 25

22.3 Mev Proton Beam
Depth in Phantom 3660 Microns
Methane Pressure 190 mm Hg
Simulated Cell Size - 2.3 Microns (spherical)
1700 Volts Bias

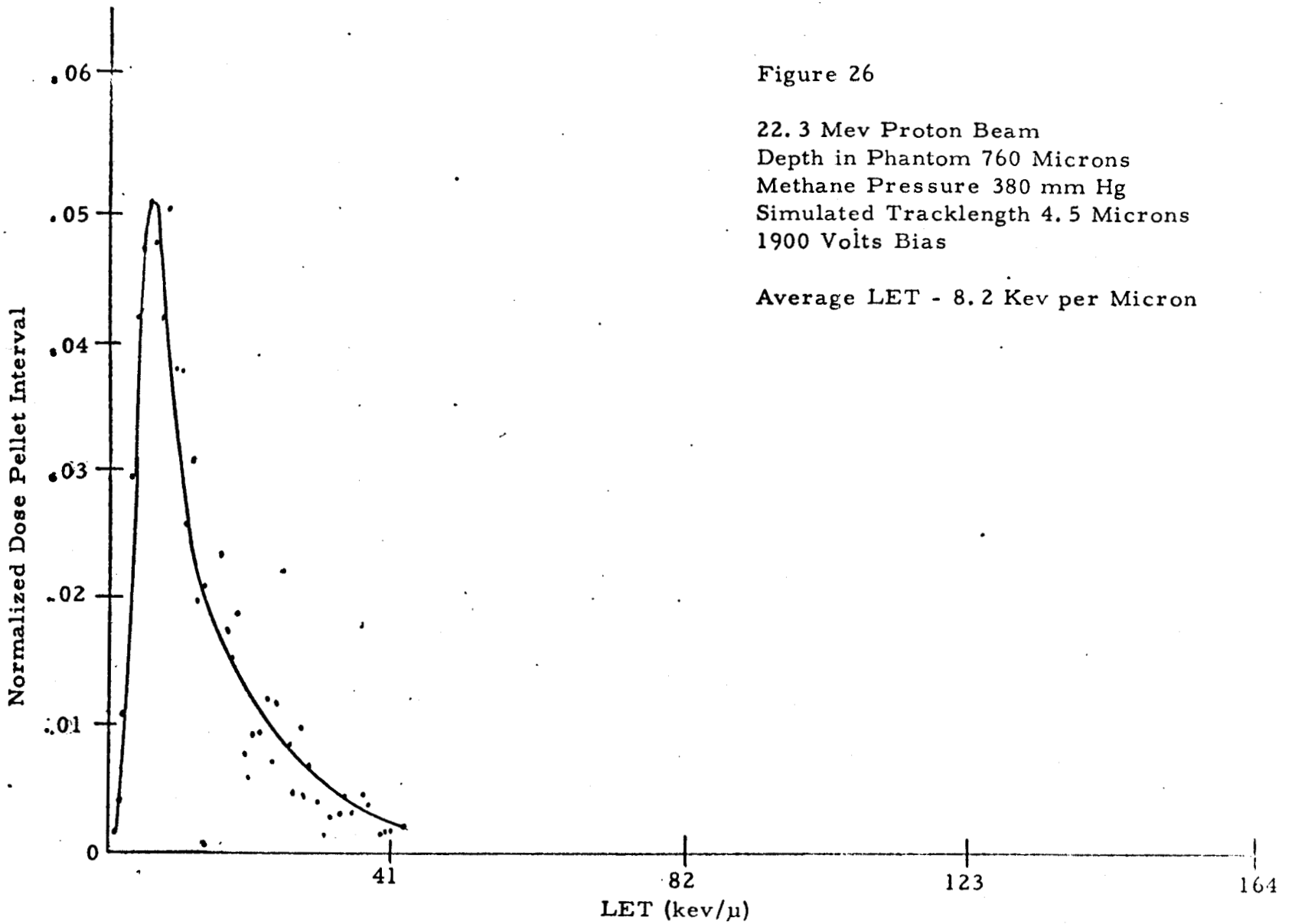

Figure 26

22.3 Mev Proton Beam
Depth in Phantom 760 Microns
Methane Pressure 380 mm Hg
Simulated Tracklength 4.5 Microns
1900 Volts Bias

Average LET - 8.2 Kev per Micron

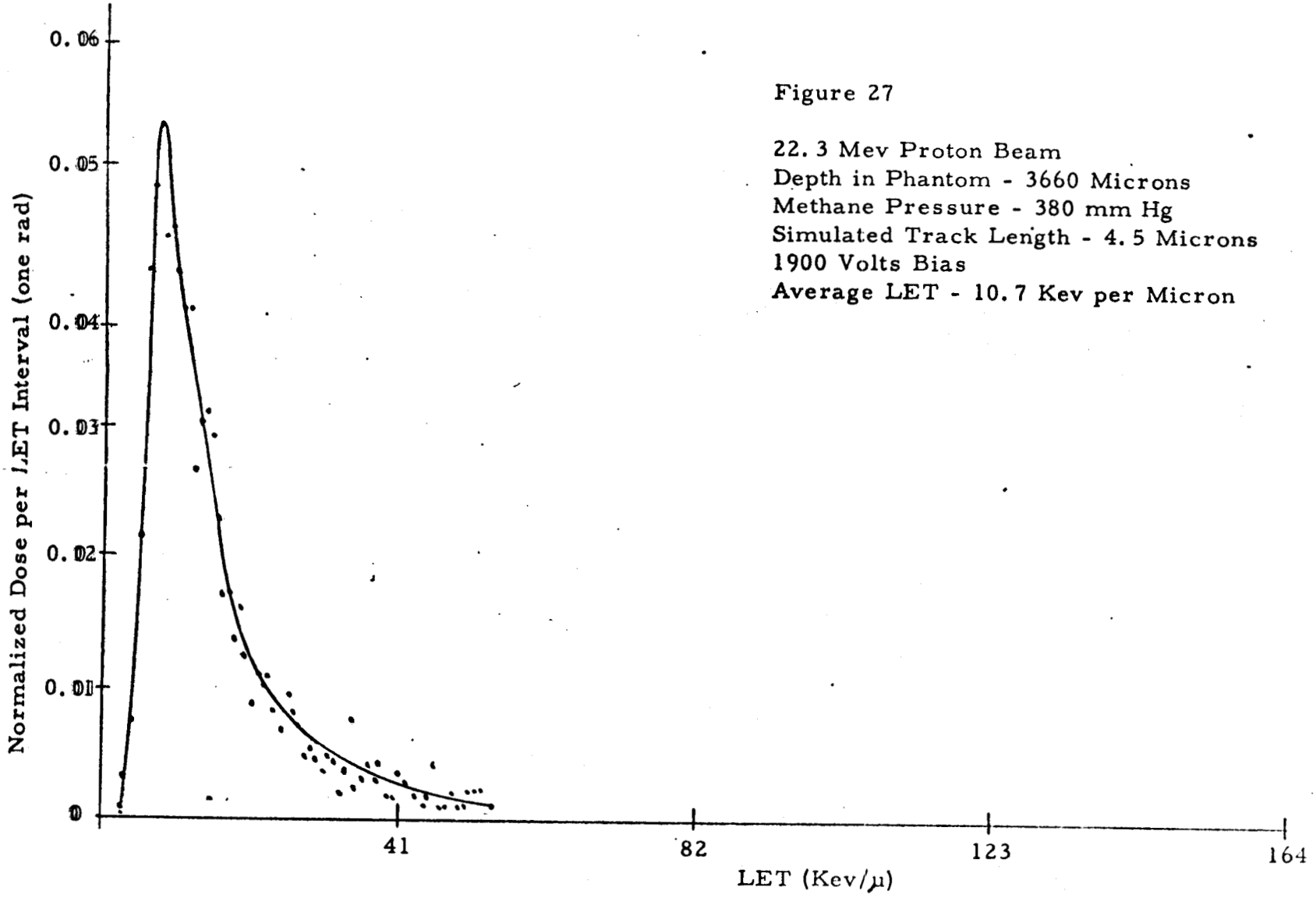

Figure 27

22.3 Mev Proton Beam
Depth in Phantom - 3660 Microns
Methane Pressure - 380 mm Hg
Simulated Track Length - 4.5 Microns
1900 Volts Bias
Average LET - 10.7 Kev per Micron

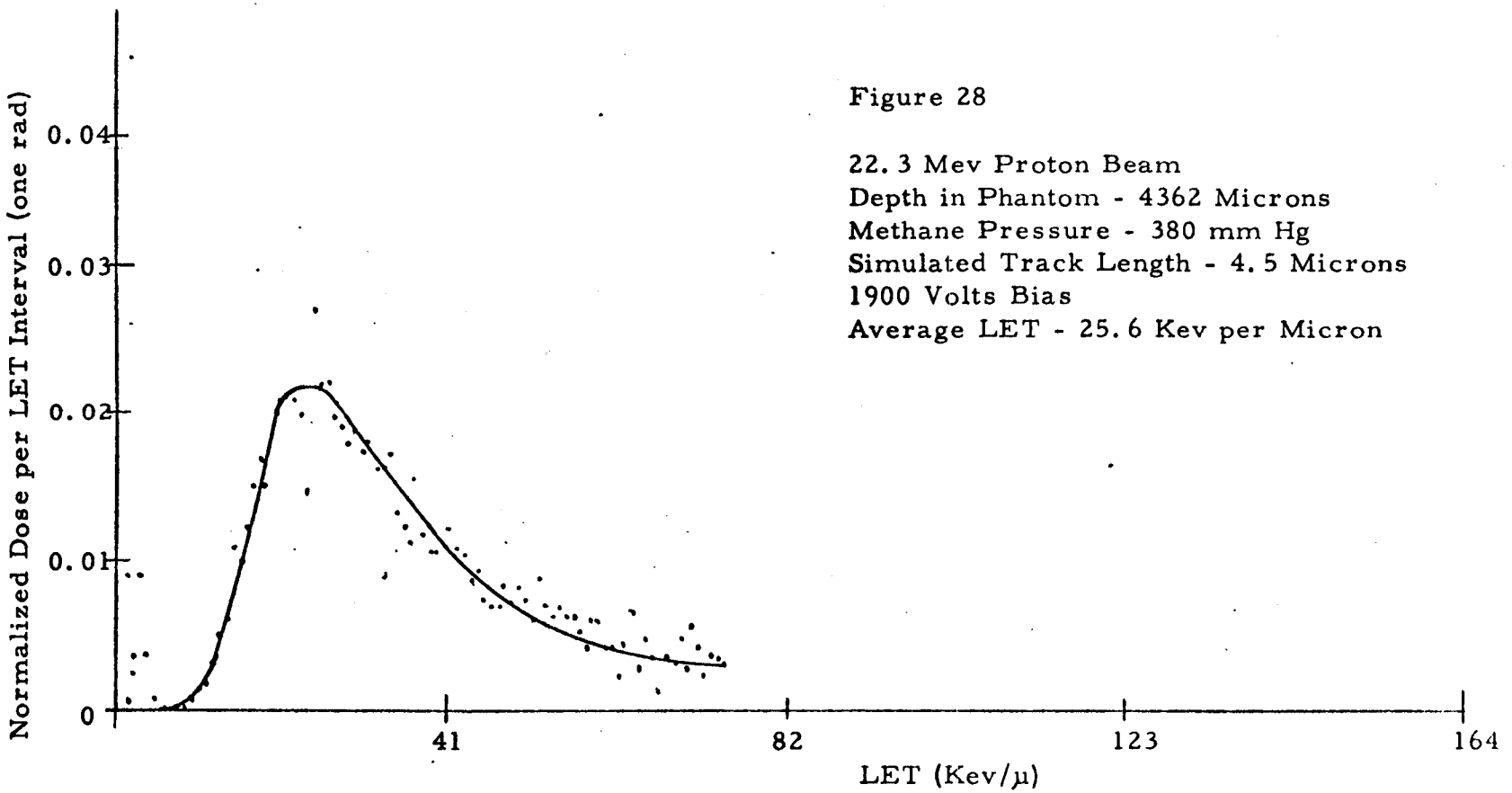

Figure 28

22.3 Mev Proton Beam
Depth in Phantom - 4362 Microns
Methane Pressure - 380 mm Hg
Simulated Track Length - 4.5 Microns
1900 Volts Bias
Average LET - 25.6 Kev per Micron

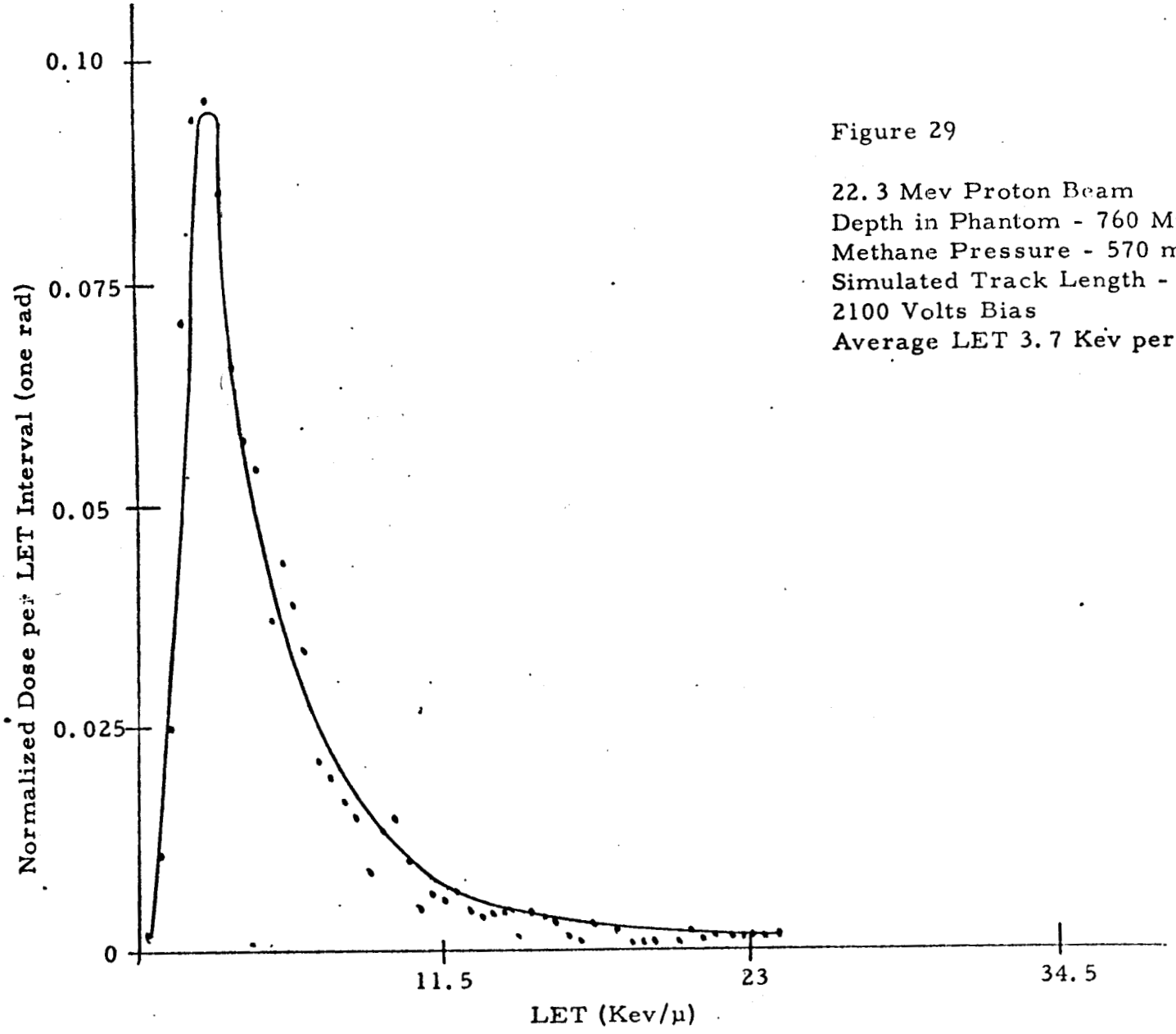

Figure 29

22.3 Mev Proton Beam
Depth in Phantom - 760 Microns
Methane Pressure - 570 mm Hg
Simulated Track Length - 6.8 Microns
2100 Volts Bias
Average LET 3.7 Kev per Micron

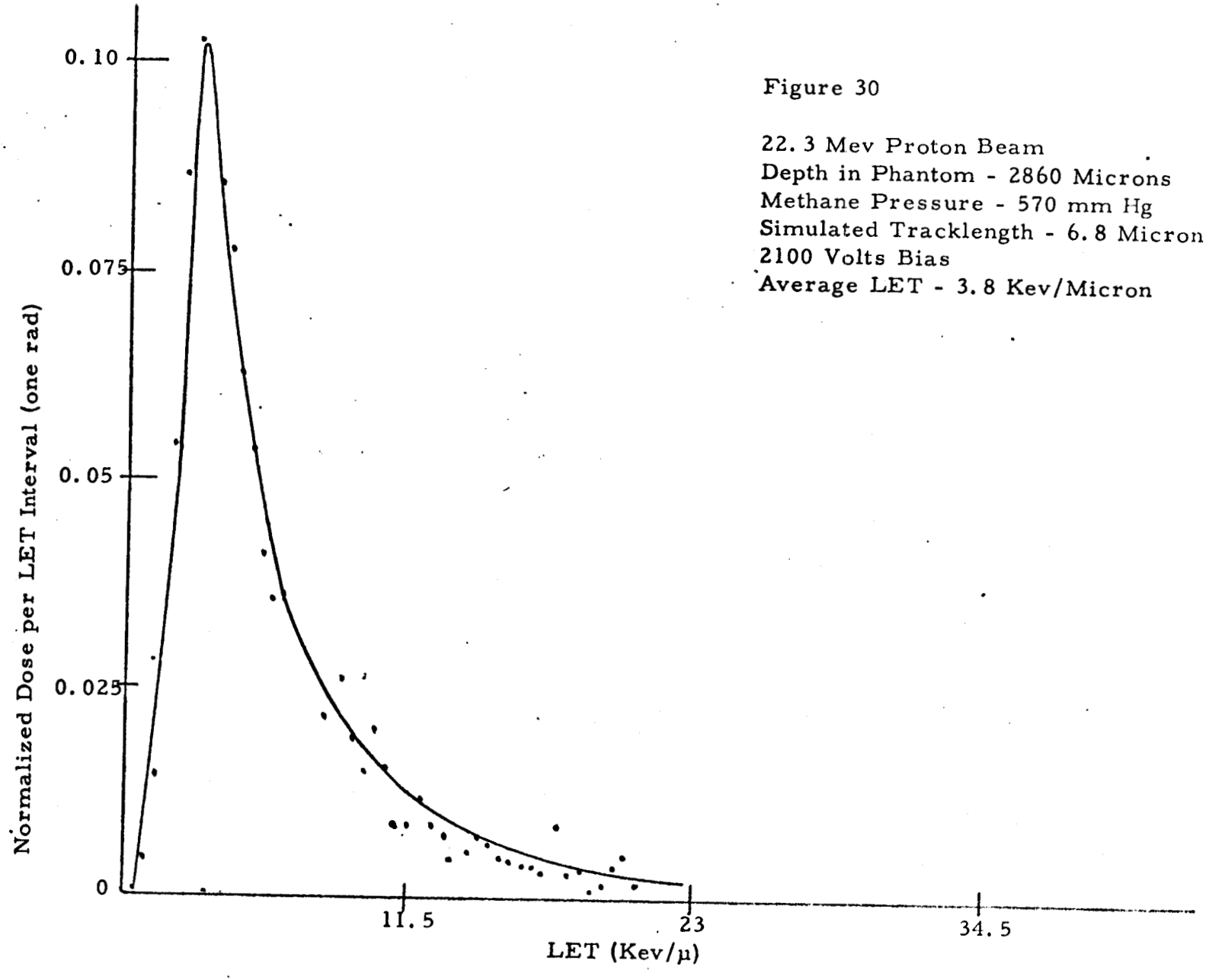

Figure 30

22.3 Mev Proton Beam
Depth in Phantom - 2860 Microns
Methane Pressure - 570 mm Hg
Simulated Tracklength - 6.8 Microns
2100 Volts Bias
Average LET - 3.8 Kev/Micron

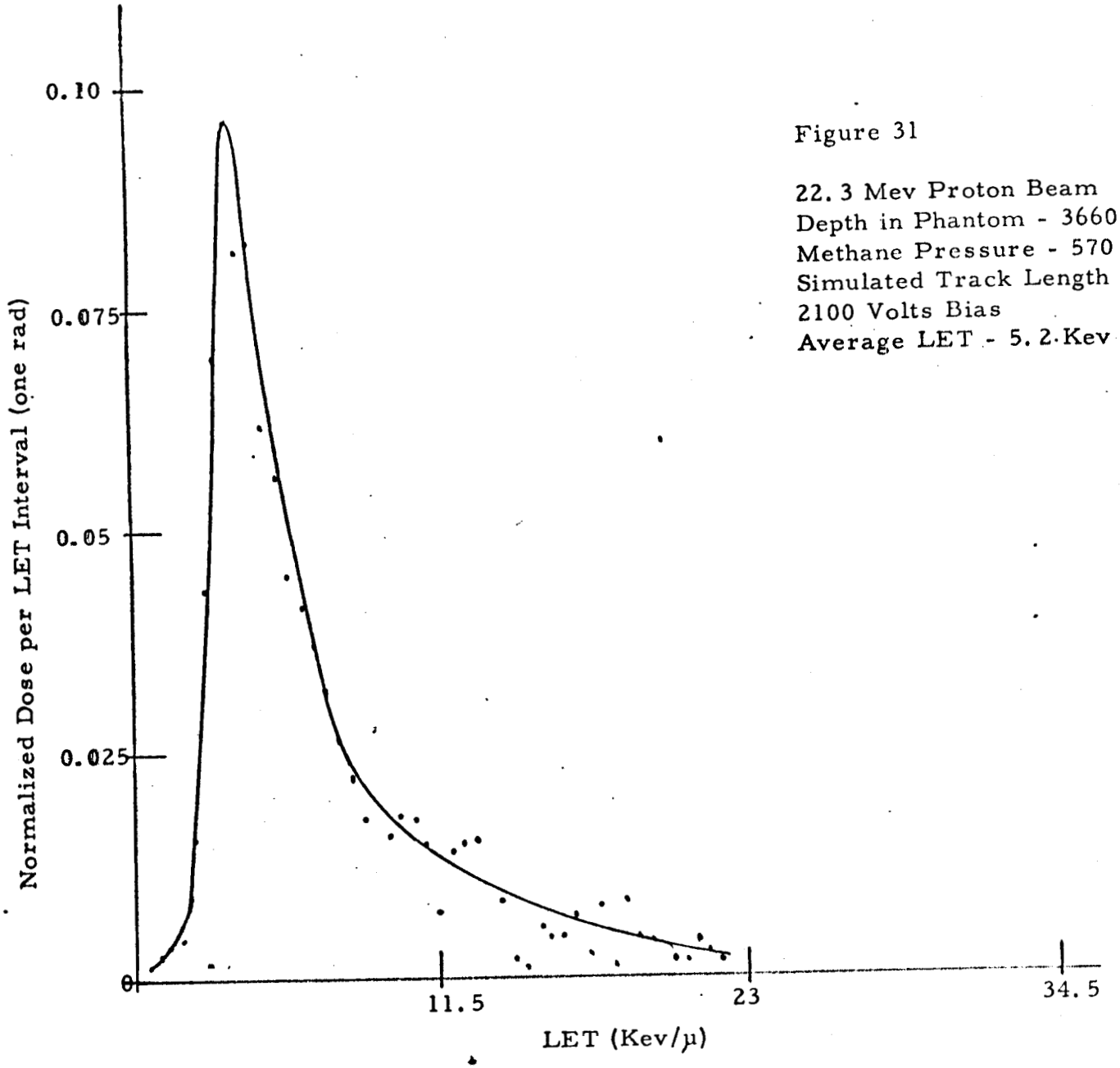

Figure 31

22.3 Mev Proton Beam
Depth in Phantom - 3660 Microns
Methane Pressure - 570 mm Hg
Simulated Track Length - 6.8 Microns
2100 Volts Bias
Average LET - 5.2 Kev per Micron

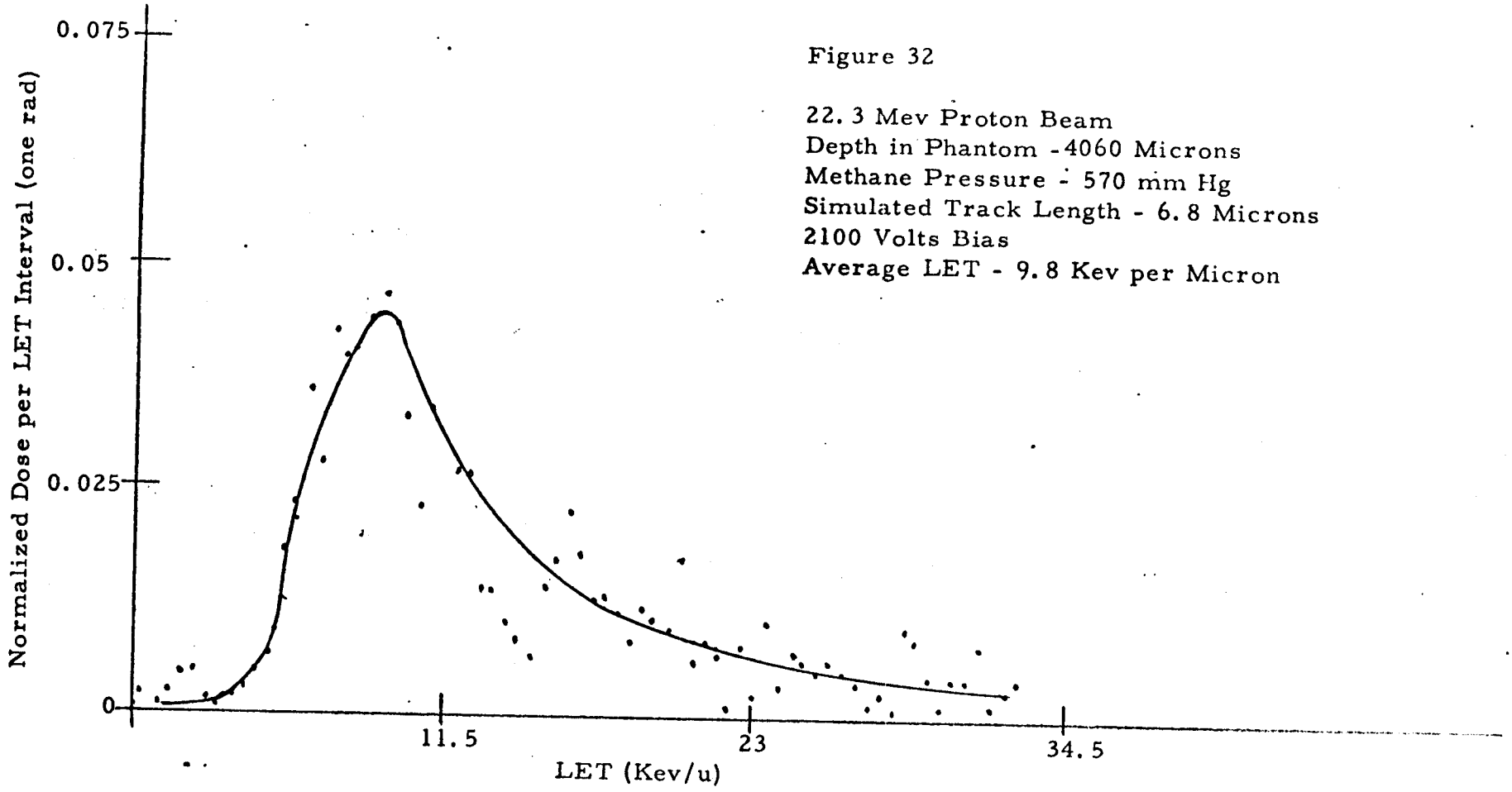

Figure 32

22.3 Mev Proton Beam
Depth in Phantom -4060 Microns
Methane Pressure - 570 mm Hg
Simulated Track Length - 6.8 Microns
2100 Volts Bias
Average LET - 9.8 Kev per Micron

Figure 33

Average LET versus Depth in Phantom
for Different Simulated Track Lengths

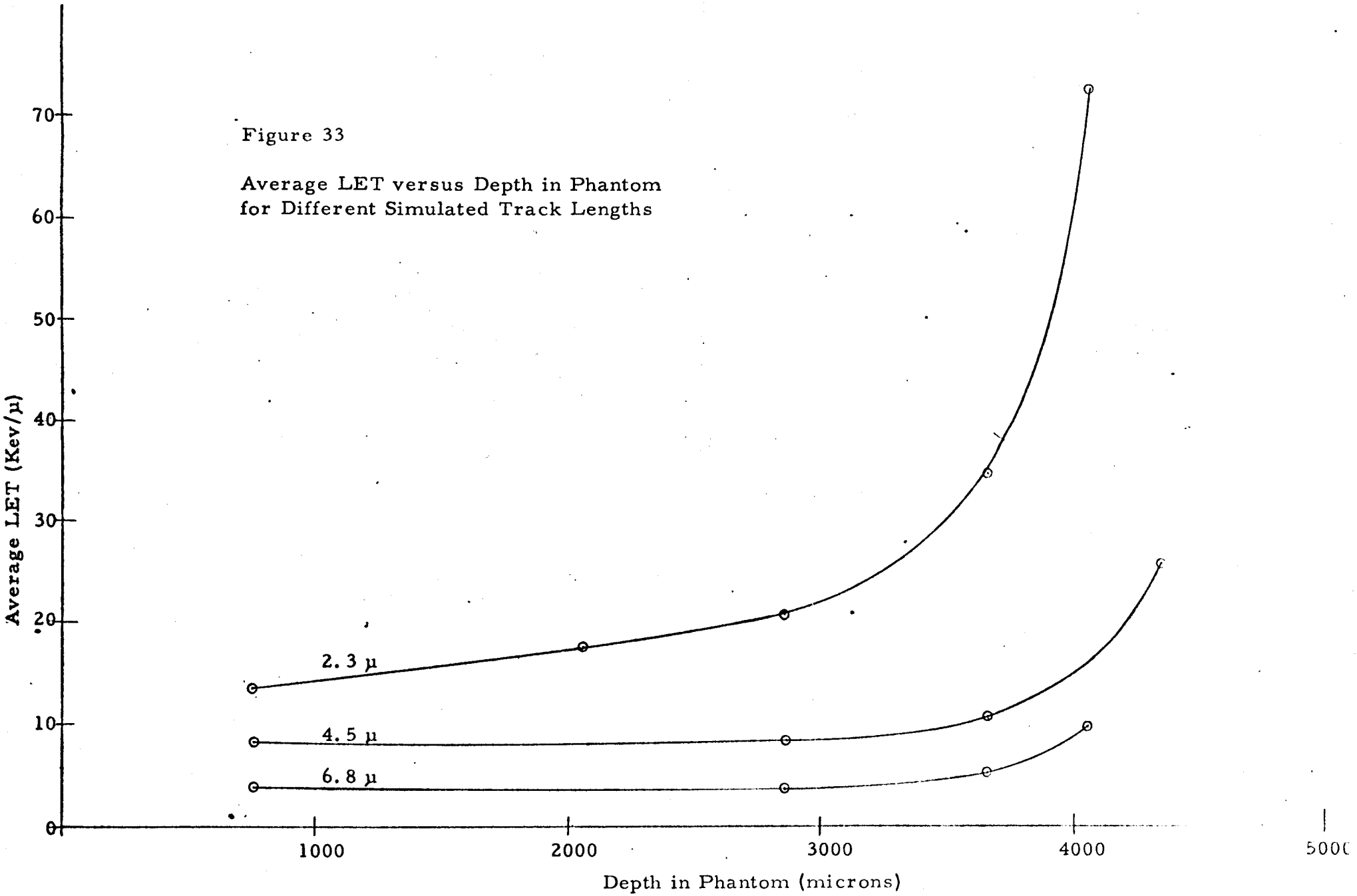

Figure 34

Killing Effect on SC-7 Yeast Cells in the Tissue Simulant by 22.5 Mev Protons

Curve I - Total Dose 1,200 rad at. Zero Microns.

Curve II - Total Dose 6,900 rad at Zero Microns

Curve III - Total Dose 13,600 rad at Zero Microns

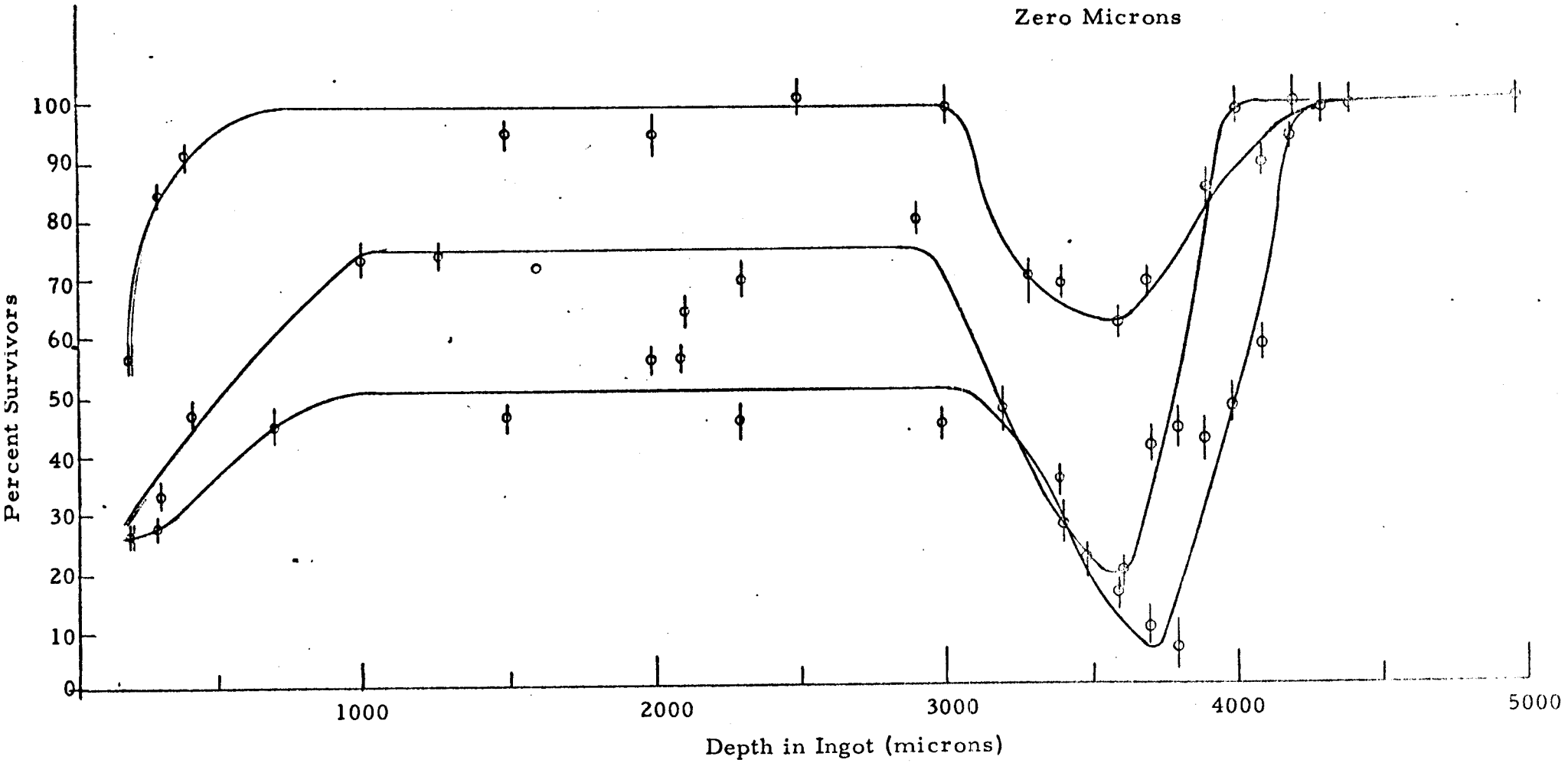

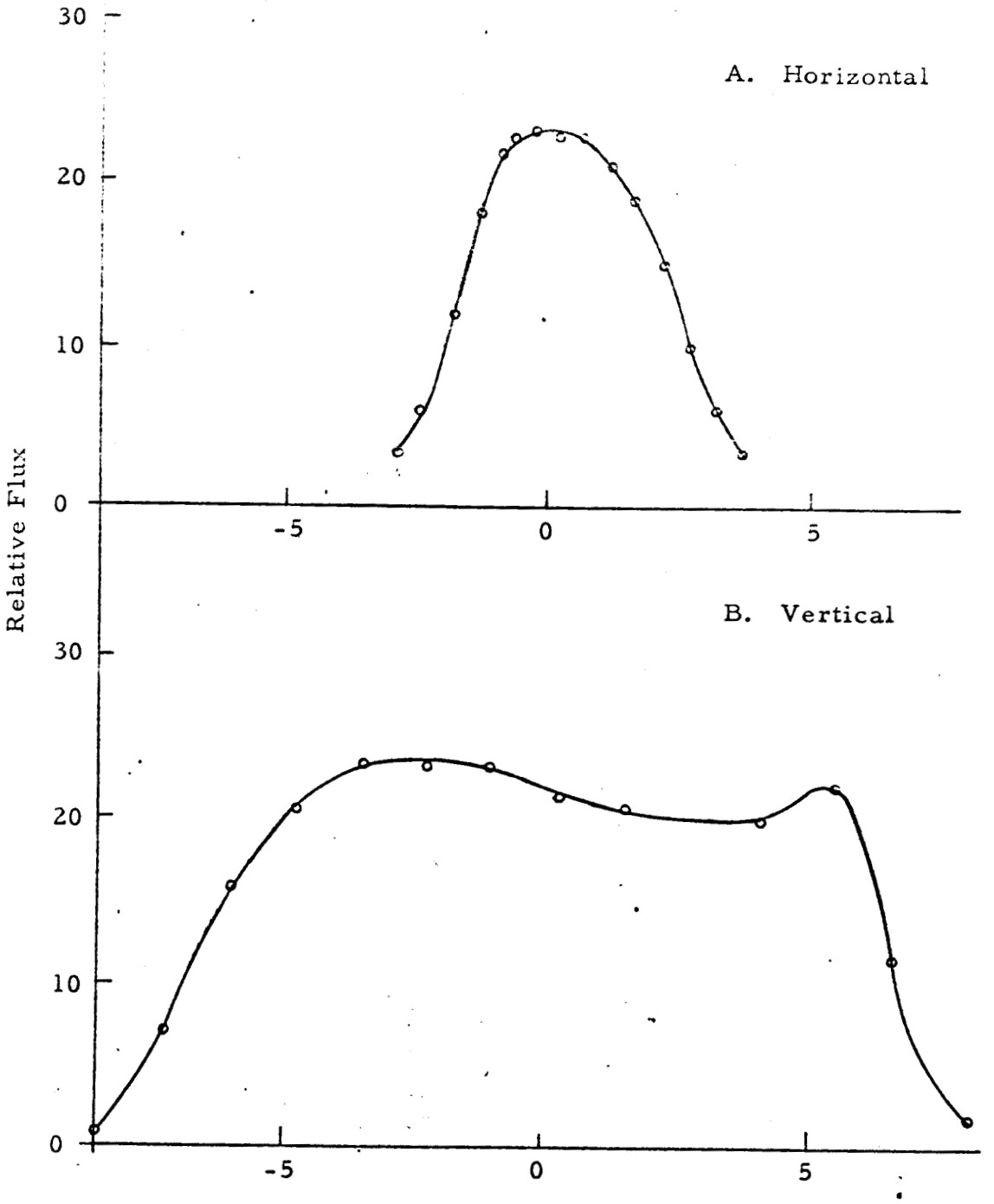

Figure 35

Distance from Center Beam, Cm.
Proton Beam Size Measured by Small Head Scintillation Counter

Figure 36

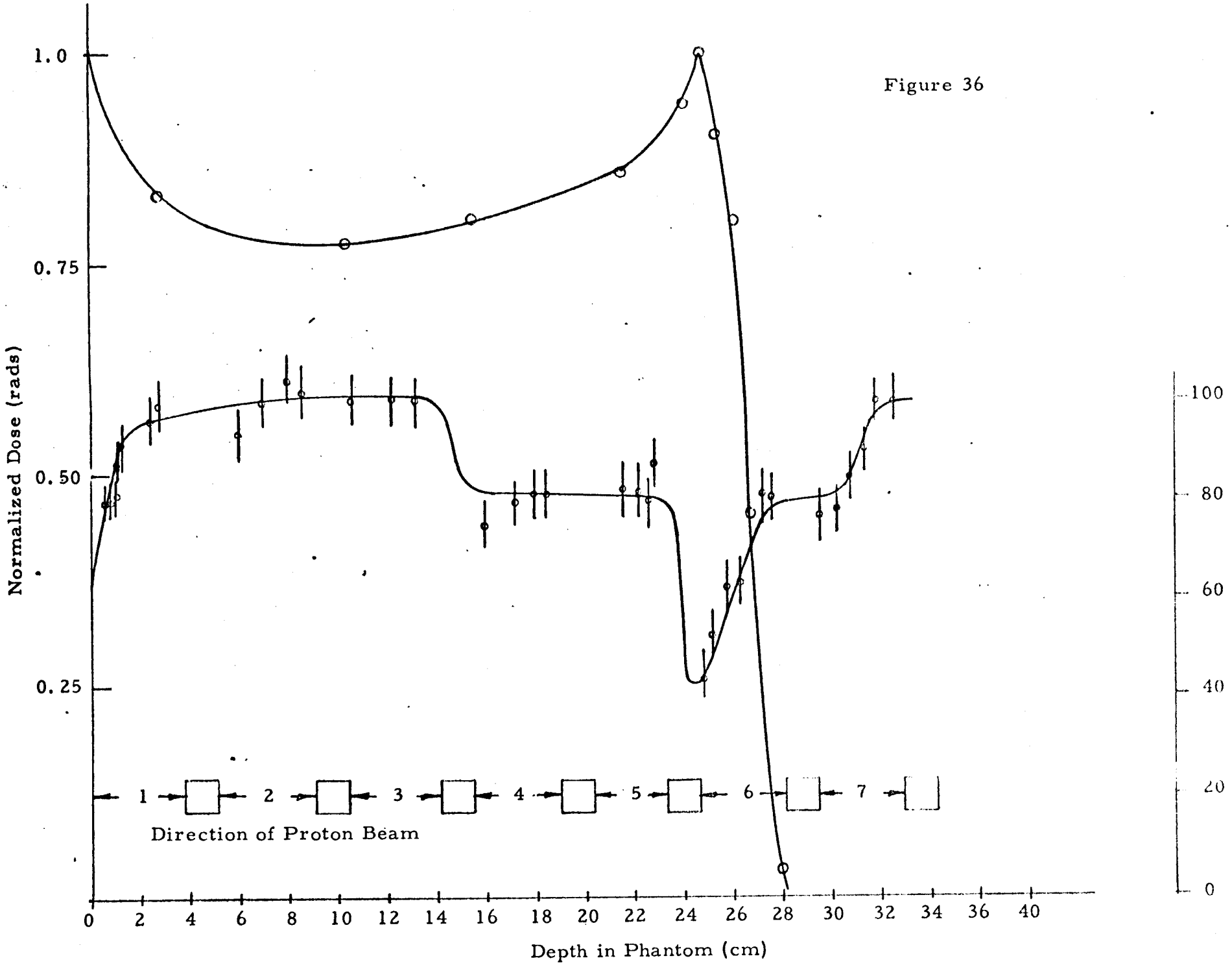
1.0
0.75
0.50
0.25
Normalized Dose (rads)
100
80
60
40
20
0
1
2
3
4
5
6
7
Direction of Proton Beam
0
2
4
6
8
10
12
14
16
18
20
22
24
26
28
30
32
34
36
40
Depth in Phantom (cm)

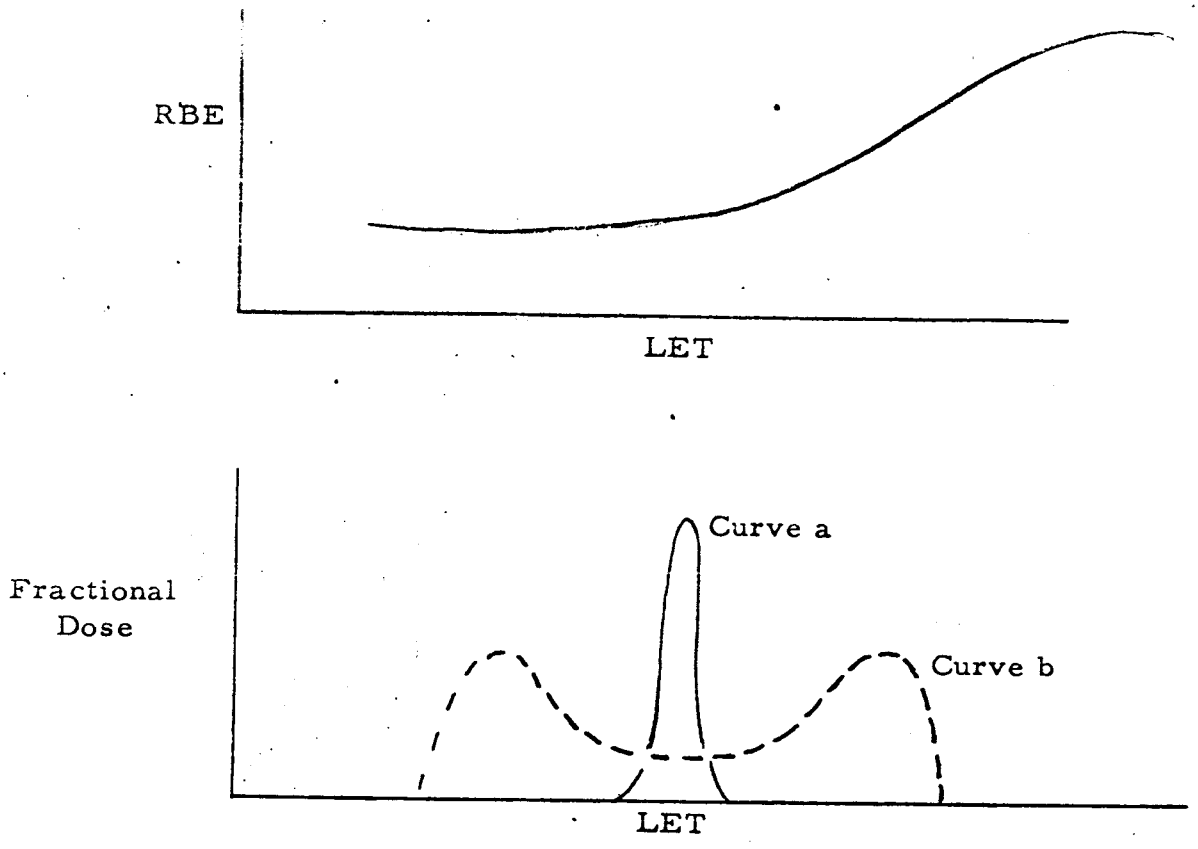

Figure 37

Illustration of Concepts Involved in Correlating LET and RBE.

REFERENCES

1. Van Dilla, M. A., J. H. Larkins, et. al. Radiation Dose Rates Above the Atmosphere. LAMS-2445, p. 157-62.

2. Contract AF 29(601)-6000 entitled "Development of Advanced Tissue-Equivalent Ion Chambers for Space Use."

3. Contract AF 29(601)-6346 entitled "Dose Rate Instrumentation for Project Gemini and Air Force Satellite Spaceflights."

4. Boag, J. W. "The Relative Biological Efficiency of Different Ionizing Radiations." National Bureau of Standards Report 2946, 1953.

5. Zirkle, R. E. "The Radiobiological Importance of Linear Energy Transfer." Radiation Biology (A. Hollander, ed.) Volume I, Chapter VI, McGraw-Hill Book Co.:N. Y., 1954.

6. Foelsche, Trutz. "Current Estimates of Radiation Doses in Space." National Aeronautics and Space Administration, Langley Research Center, Langley Field, Virginia, July 1962, 51 p. (NASA-TN-D1267).

7. Rossi, H. H. "Specification of Radiation Quality." Radiation Research 10, 522-31, 1959.

8. Shonka, F. R., et. al. "Conducting Plastic Equivalent to Tissue, Air and Polystyrene." Progress in Nuclear Energy Health Physics, p. 160, Pergamon Press, 1958.

9. Humbel, F. and A. Stebler. "Dosimeter with Tissue-Equivalent Ionization Chamber." p. 589-93 of "Selected Topics in Radiation Dosimetry." Vienna, International Atomic Energy Agency, 1961.

10. Hine, G. J. and G. L. Brownell. "Radiation Dosimetry." Academic Press Inc., 1956.

11. Myers, I. T. "The Measurement of the Electron Energy Required to Produce an Ion Pair in Various Gases." Ph. D. Thesis, State College of Washington, 1958.

12. Tanooka, H. "Inactivation of Bacteriophage T6 in an Aqueous System by High-Energy Protons." AEC Research and Development Report UR-618, 1962.

13. Barendsen, G. W. and T. L. Bensker. "Effects of Different Ionizing Radiations on Human Cells in Tissue Culture." Radiation Research 13, 832-40, 1960.

14. Tobias, C. A. "The Dependence of some Biological Effects of Radiation on the Rate of Energy Loss." In Symposium on Radiobiology (J. J. Nickson, ed.), pp. 357-84, John Wiley and Sons, Inc.: N. Y., 1960.

15. Dewey, D. L. "Effect of Glycerine on X-Ray Sensitivity of Serratia marcescens." Nature 187, 1008-10, 1960.

16. Mookerjee, A. "Effects of X-irradiation on Survival of Yeast in Dry and Wet Conditions." Nature 184, 1502-3, 1959.

17. Sayeg, J. A. and A. C. Birge. "Relative Biological Effectiveness of Various Ionizing Radiations on Yeast Cells." Radiation Research, 1, 560, 1954.

18. Laser, H. "Influence of Oxygen on Radiation Effects." Cuba Foundation Symposium, pp. 106-19, 1956.

19. Sayeg, J. A., A. C Birge, C. A. Beam, and C. A. Tobias. "The Effects of Accelerated Carbon Nuclei and Other Radiations on the Survival of Haploid Yeast." Radiation Research, 10, 449-61, 1959.